VPS35 haploinsufficiency increases Alzheimer's disease neuropathology

Lei Wen,[1,2] Fu-Lei Tang,[1,2] Yan Hong,[1,2] Shi-Wen Luo,[1,2] Chun-Lei Wang,[1,2] Wanxia He,[3] Chengyong Shen,[1,2] Ji-Ung Jung,[1,2] Fei Xiong,[1,2] Dae-hoon Lee,[1,2] Quan-Guang Zhang,[1,2] Darrell Brann,[1,2] Tae-Wan Kim,[4,5] Riqiang Yan,[3] Lin Mei,[1,2] and Wen-Cheng Xiong[1,2]

[1]Institute of Molecular Medicine and Genetics and [2]Department of Neurology, Medical College of Georgia, Georgia Health Sciences University, Augusta, GA 30912
[3]Department of Neurosciences, Lerner Research Institute, Cleveland Clinic, Cleveland, OH 44195
[4]Department of Pathology and Cell Biology and [5]Taub Institute for Research on Alzheimer's Disease and the Aging Brain, Columbia University Medical Center, New York, NY 10032

VPS35, a major component of the retromer complex, is important for endosome-to-Golgi retrieval of membrane proteins. Although implicated in Alzheimer's disease (AD), how VPS35 regulates AD-associated pathology is unknown. In this paper, we show that hemizygous deletion of Vps35 in the Tg2576 mouse model of AD led to earlier-onset AD-like phenotypes, including cognitive memory deficits, defective long-term potentiation, and impaired postsynaptic glutamatergic neurotransmission in young adult age. These deficits correlated well with an increase of β-amyloid peptide (Aβ) level in the mutant hippocampus. We further demonstrate that VPS35 is predominantly expressed in pyramidal neurons of young adult hippocampus and interacts with BACE1, a protease responsible for Aβ production. Loss of VPS35 function in the mouse hippocampus increased BACE1 activity. Suppression of VPS35 expression in culture decreased BACE1 trans-Golgi localization but enriched it in endosomes. These results demonstrate an essential role for VPS35 in suppression of AD neuropathology and in inhibition of BACE1 activation and Aβ production by promoting BACE1 endosome-to-Golgi retrieval.

Introduction

Aβ, a 40–42 peptide released from amyloid precursor protein (APP) after the sequential cleavages by β- and γ-secretases, is recognized as a major culprit of Alzheimer's disease (AD), the most common dementia in people >65 yr of age. Cortical and cerebral vascular Aβ deposition is a pathological hallmark in AD, in addition to neurofibrillary tangles, chronic inflammation, and neuronal loss (Tanzi and Bertram, 2005). Mutations in the genes of APP and presenilin, an essential component of γ-secretase, are found in the early-onset AD. Many risk factors or genes associated with the late-onset AD also affect APP protein metabolism and Aβ production (Tanzi and Bertram, 2005). Multiple forms of Aβ have been reported, but the prefibrillar and/or soluble oligomers of Aβ, not Aβ deposits, have been recognized to be early and key intermediates in AD-related synaptic dysfunction (Walsh et al., 2005; Smith et al., 2007; Stefani and Liguri, 2009). Mouse brain slices exposed to soluble Aβ oligomers exhibit synaptic depression, decrease of the number of spine protrusions or synaptic contacts, and impaired long-term potentiation (LTP), a form of synaptic plasticity (Roselli et al., 2005; Townsend et al., 2006; Nimmrich et al., 2008; Selkoe, 2008; Li et al., 2009). In addition, synaptic function is disrupted, and synapses are lost in AD patients and in animal models even before amyloid plaques are detected (Selkoe, 2002a, 2008; Ashe and Zahs, 2010). Collectively, these lines of evidence from pathological, genetic, biochemical, and physiological studies have indicated a crucial role of Aβ in the etiology of AD.

Extensive efforts have been invested to the understanding of Aβ production. β-secretase, also called BACE1, is essential

L. Wen and F.-L. Tang contributed equally to this paper.

Correspondence to Wen-Cheng Xiong: wxiong@georgiahealth.edu

Abbreviations used in this paper: aCSF, artificial cerebrospinal fluid; AD, Alzheimer's disease; ANOVA, analysis of variance; APP, amyloid precursor protein; DG, dentate gyrus; DIV, day in vitro; eEPSC, evoked excitatory postsynaptic current; eIPSC, evoked inhibitory postsynaptic current; ES, embryonic stem; fEPSP, field excitatory postsynaptic potential; LTP, long-term potentiation; mEPSC, miniature EPSC; mIPSC, miniature IPSC; miRNA, microRNA; NMDA, *N*-methyl D-aspartate; PD, Parkinson's disease; SC, Schaffer collateral; shRNA, small hairpin RNA; WT, wild type.

The Rockefeller University Press $30.00
J. Cell Biol. Vol. 195 No. 5 765–779
www.jcb.org/cgi/doi/10.1083/jcb.201105109

for this event (Hussain et al., 1999; Sinha et al., 1999; Vassar et al., 1999, 2009; Yan et al., 1999; Tanzi and Bertram, 2005; Bertram and Tanzi, 2008). BACE1 activity is increased in postmortem brains of AD patients and in brains of AD mouse models (Fukumoto et al., 2002; Yang et al., 2003). Genetic ablation of BACE1 in AD animals abolishes Aβ production and rescues AD-like phenotypes (Luo et al., 2001; Ohno et al., 2004; Laird et al., 2005). BACE1 is a type I transmembrane aspartyl protease that has a broad substrate profile, including sialyltransferase, P-selectin glycoprotein ligand 1, sodium channel, and APP-like proteins, in addition to APP (Vassar et al., 2009). An in vitro study has suggested that the optimal pH of BACE1-mediated APP cleavage is pH ∼5.0, suggesting that an acidic intracellular compartment (e.g., endosome) may be more favorable for BACE1 activation (He et al., 2003). After the cleavage by BACE1, γ-secretase—a multimeric complex that contains presenilins, nicastrin, aph-1, and pen2—cleaves the membrane-anchored C-terminal fragment of APP to release $A\beta_{40/42}$ (Selkoe and Wolfe, 2007). Genetic mutations surrounding the γ-cleavage sites in APP can alter the ratio of $A\beta_{40}$ versus more toxic and amyloidogenic $A\beta_{42}$ (Selkoe and Wolfe, 2007). Mutations in presenilin genes in the early-onset AD patients may cause a gain of function of γ-secretase, leading to the increase in $A\beta_{42}$ to $A\beta_{40}$ ratio (Selkoe, 2002b; Sisodia and St George-Hyslop, 2002). Finally, APP can also be cleaved by α-secretases, including ADAM10, that switch APP processing to a nonamyloidogenic pathway and thus reduce the $A\beta_{40/42}$ production (Esler and Wolfe, 2001).

The retromer contains two subprotein complexes: the cargo-selective subcomplex and membrane deformation subcomplex (Seaman, 2005; Bonifacino and Hurley, 2008). The cargo-selective complex is a trimer of vacuolar protein sorting (Vps) proteins VPS35, VPS29, and VPS26 that sorts cargos into tubules for retrieval to the Golgi apparatus. The membrane deformation subcomplex, consisting of sorting nexin dimers (Vps5p and Vps17p in yeast and sortin nexins 1/3 or 5/6 in vertebrates), deforms the donor membrane into a tubular profile (Seaman, 2005; Bonifacino and Hurley, 2008; van Weering et al., 2010). The retromer selectively mediates retrograde transport of multiple transmembrane proteins from the endosomes to the TGN. They include mannose 6-phosphate receptors (Arighi et al., 2004), wntless (a receptor for Wnt morphogens; Belenkaya et al., 2008; Eaton, 2008; Franch-Marro et al., 2008; Pan et al., 2008; Port et al., 2008; Yang et al., 2008), Ced1 (a phagocytic receptor; Chen et al., 2010), and VPS10 family proteins, such as VPS10 in yeast (Iwaki et al., 2006), sortilin, and sortilin-related receptor (SorL1 or SorCS1) in vertebrates (Canuel et al., 2008; Kim et al., 2010; Okada et al., 2010). Recent studies have suggested that SorL1, also called SorLA and LR11, is an APP-binding protein and is involved in the pathogenesis of late-onset AD (Rogaeva et al., 2007; Willnow et al., 2010). In addition, the cargo-selective retromer proteins VPS35 and VPS26 are decreased in the postmortem hippocampus of AD patients (Small et al., 2005). Moreover, VPS26 heterozygote mice show increased levels of endogenous Aβ and impaired LTP (Muhammad et al., 2008). These observations suggest that the retromer may be involved in the AD pathogenesis. However, the underlying mechanisms remain elusive.

To elucidate functions of the retromer in AD pathogenesis, we crossed Tg2576 mice, a well-established AD mouse model that expresses the Swedish mutant form of human APP (APPswe) under the control of prion promoter (Chapman et al., 1999; Rockenstein et al., 2007), with Vps35 mutant mice. Vps35 homozygous mutant mice died during early embryonic development, but heterozygotes can survive into adulthood with relatively normal behavior, synaptic plasticity, and life span. Remarkably, Vps35 heterozygotes;Tg2576 mice demonstrated an earlier onset of AD-like neuropathology, including cognitive deficits, impaired glutamatergic transmission, and synaptic plasticity, and more Aβ-positive plaques detected in the brain. These earlier-onset AD-like phenotypes in the double mutant mice suggest that reduced VPS35 levels may exacerbate Aβ toxicity. We have investigated underlying mechanisms, and our results suggest that VPS35 is required for the endosome-to-Golgi retrieval of BACE1.

Results

Genetic enhancement and earlier onset of Tg2576-associated cognitive deficit by loss of VPS35 function

Defective spatial learning and memory are known to be early symptoms of AD (Middei et al., 2006; Bizon et al., 2007; Good and Hale, 2007; Reed et al., 2010). They are also observed in 8-mo or older Tg2576 mice that express APPswe (Hsiao et al., 1996; Chapman et al., 1999; Rockenstein et al., 2007). To study the potential role of VPS35 in AD pathology, we generated Vps35-deficient mice by using gene-trapping embryonic stem (ES) cells from Bay Genomics (see Materials and methods; Fig. S1 A). Homozygotes, named $Vps35^{m/m}$, were lethal at an early embryonic stage (under embryonic day 10 [E10]), but heterozygotes, named $Vps35^{+/m}$, whose expression of Vps35 was ∼50% of that in wild type (WT; Fig. S1 B), survived to adulthood. We crossed $Vps35^{+/m}$ mice with Tg2576 mice to generate $Vps35^{+/m}$;$Tg2576^{+/-}$ mice (Fig. S1 B) and subjected them and control littermates (WT, $Tg2576^{+/-}$ and $Vps35^{+/m}$) to the Morris water maze test to assess their spatial learning and memory (Morris, 1991). In this assay, 3- and 6-mo-old mice were dropped into a pool and allowed to swim to locate a submerged platform to escape swimming. Tg2576 and $Vps35^{+/m}$ mice had normal spatial learning and memory response as compared with the age-matched WT control in viewing their learning the location of the submerged platform with repeated testing (Fig. 1). However, the double mutant ($Tg2576^{+/-}$;$Vps35^{+/m}$) mice were impaired in this task, exhibiting increases of latencies in finding the hidden platform (Fig. 1, A and B) and in pathway length (Fig. 1, C and D) as compared with the other three age-matched groups. In addition, $Tg2576^{+/-}$;$Vps35^{+/m}$ mutant mice performed worse than all other groups in probe trials, with less frequency to probe the hidden platform (Fig. 1, E and F). Note that no significant difference was observed in velocity among the four groups (Fig. 1, G and H). Intriguingly, deficits of $Tg2576^{+/-}$;$Vps35^{+/m}$ mice in latency and distance and platform probe frequency appeared to be severer in 6-mo-old $Tg2576^{+/-}$;$Vps35^{+/m}$ mice compared with those in 3-mo-old (Fig. 1, A–F). Moreover, double mutant mice at 1–2 mo

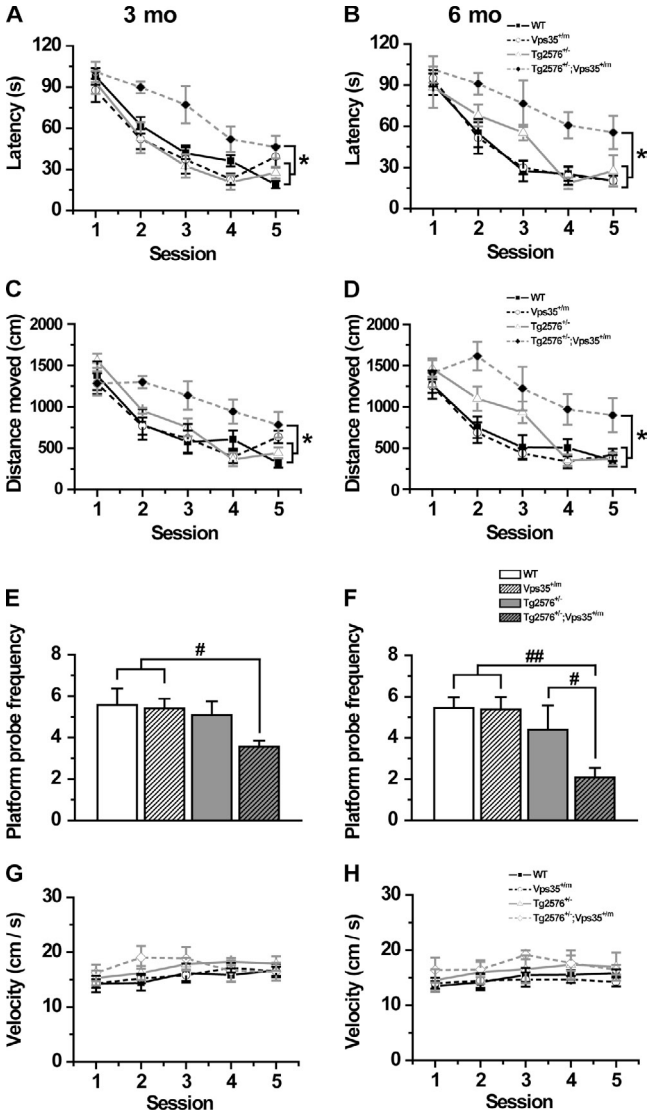

Figure 1. **Impaired spatial learning and memory by the Morris water maze test in young adult Tg2576$^{+/-}$;Vps35$^{+/-}$ mice.** (A–H) 3 (A, C, E, and G)- and 6 (B, D, F, and H)-mo-old Tg2576$^{+/-}$;Vps35$^{+/m}$ mice showed increases of swimming latency (A and B) and total distance (C and D) in the training sessions but decreases of the platform probe frequency (E and F) in the probe tests relative to the age-matched Tg2576$^{+/-}$, Vps35$^{+/m}$, and nontransgenic (WT) mice. Although Tg2576$^{+/-}$;Vps35$^{+/m}$ showed slightly higher velocity at day 1–3 sessions, repeated measures ANOVA analysis of the total five sessions showed no significant change of the velocity among the four groups in both 3- and 6-mo-old mice (G and H). Comparing the performance between 3- and 6-mo-old Tg2576$^{+/-}$;Vps35$^{+/m}$ mice, a trend toward longer latency and distance was noted in the 6-mo-old mice, but the difference was not significant ($P > 0.05$, using repeated measures ANOVA). However, the platform probe frequency was significantly reduced in 6-mo-old Tg2576$^{+/-}$;Vps35$^{+/m}$ mice as compared with that in 3-mo-old ($P < 0.05$). Data shown are mean ± SEM, and $n = 6$–10 for each of the genotypes in 3-mo-old mice, whereas $n = 5$–11 for each of the genotypes in 6-mo-old mice. *, $P < 0.05$, with a significant difference from the Tg2576$^{+/-}$, Vps35$^{+/m}$, and WT control mice by repeated measures ANOVA; #, $P < 0.05$; ##, $P < 0.01$, with a significant difference by one-way ANOVA followed by the least significant difference test.

old did not exhibit significant impairment (unpublished data). Thus, these results demonstrate an impaired spatial learning and memory in the double mutant mice at the age of 3 and 6 mo old, suggesting an earlier onset of Tg2576-associated cognitive deficit by loss of VPS35 function.

Acceleration of Tg2576-associated synaptic plasticity and glutamatergic transmission phenotypes by loss of VPS35 function

Tg2576 mice began to show impaired LTP and synaptic transmission in dentate gyrus (DG) at 4–5 mo or older (Jacobsen et al., 2006). In the Schaffer collateral (SC) pathway (SC-CA1), the deficiency was not detectable until 12–18 mo old (Chapman et al., 1999; Fitzjohn et al., 2001). We first examined the basal synaptic function at SC-CA1 synapses and DG in hippocampal slices of 2–4-mo-old mice. Field excitatory postsynaptic potentials (fEPSPs) were recorded in the CA1 stratum radiatum or in the stratum moleculare of the DG by stimulating the SC/commissural pathway (for CA1) or the perforant pathway (for DG) at various intensities. No significant difference in fEPSP slopes was detected at the tested stimulus intensities in both CA1 and DG areas of Tg2576, Vps35$^{+/m}$, and their WT littermate controls (Fig. 2, A and B), suggesting similar strength of basal synaptic transmission. However, the fEPSP slopes in both CA1 and DG were reduced in Tg2576$^{+/-}$;Vps35$^{+/m}$ hippocampal slices compared with those of WT, Tg2576, or Vps35$^{+/m}$ mice (Fig. 2, A and B), indicating that synaptic transmission is more vulnerable in Tg2576 mice when VPS35 level was reduced. Next, we determined whether VPS35 reduction alters synaptic plasticity by measuring LTP at the SC-CA1 synapses and DG. The posttetanic potentiation of synaptic transmission (within 3 min of tetanic stimulation initiation) was similar in CA1 2-mo-old hippocampal slices of all four groups (WT, Vps35$^{+/m}$, Tg2576, or Vps35$^{+/m}$;Tg2576$^{+/-}$) of mice. However, LTP was reduced in the double mutant (Fig. 2, C and D), suggesting impaired synaptic plasticity in CA1 in the 2-mo-old Vps35$^{+/m}$;Tg2576$^{+/-}$ hippocampus. The impairment worsened in 4-mo-old hippocampal slices in the CA1 area (Fig. 2, E and F). Both the posttetanic potentiation and LTP were reduced in 4-mo-old Vps35$^{+/m}$;Tg2576$^{+/-}$ CA1 hippocampus (Fig. 2, E and F). Note that posttetanic potentiation and LTP in the CA1 area were apparently normal in Tg2576 hippocampal slices at both ages, which is in agreement with previous reports that LTP was not impaired until at the age of >12 mo old (Chapman et al., 1999; Fitzjohn et al., 2001). In addition, LTP at the DG was defective in Tg2576$^{+/}$;Vps35$^{+/m}$ mice compared with that in WT, Tg2576$^{+/-}$, or Vps35$^{+/m}$ mice (Fig. 2, G and H). These results demonstrated that loss of Vps35 function accelerates the development of synaptic plasticity deficits in both CA1 and DG hippocampus of Tg2576 mice.

To investigate possible underlying mechanisms, we studied the excitatory and inhibitory synaptic transmission in CA1 pyramidal neurons of 2-mo-old hippocampus (Fig. 3). α-Amino-3-hydroxy-5-methyl-4-isoxazolepropionic acid (AMPA) and *N*-methyl D-aspartate (NMDA) receptor-mediated miniature excitatory postsynaptic currents (mEPSCs) were recorded in whole-cell configuration (Fig. 3, A and B). Both amplitudes of AMPA and NMDA receptor-mediated mEPSCs were significantly reduced in the CA1 pyramidal neurons from Tg2576$^{+/-}$;Vps35$^{+/m}$ mutant mice as compared with the other three groups (Fig. 3, A–D). These results indicate a defective glutamatergic transmission in postsynaptic regions of the double mutant hippocampus. Interestingly, we also observed reductions of the frequencies of

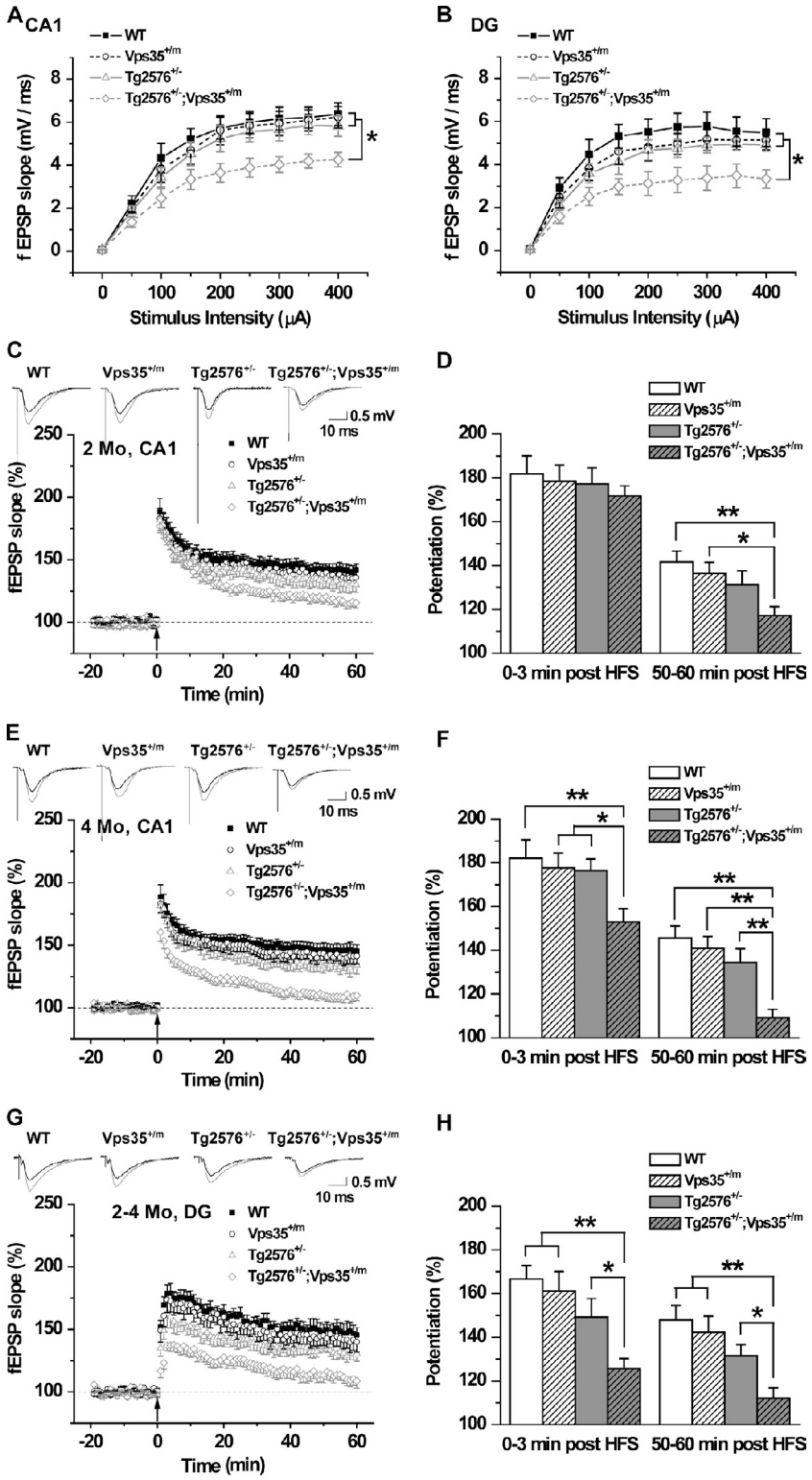

Figure 2. **Acceleration of LTP deficit in the CA1 region and the DG in Tg2576$^{+/-}$ hippocampus by loss of Vps35 function.** (A and B) Input–output relations generated by stimulating the SCs and recording in CA1 stratum radiatum (A) or by stimulating the perforant pathway and recording in stratum moleculare of the DG (B). The basal transmission in both CA1 (A) and DG (B) were similar in aged-matched WT, Tg2576$^{+/-}$, and Vps35$^{+/m}$ mice but was significantly impaired in Tg2576$^{+/-}$;Vps35$^{+/m}$ mice. Means ± SEM are shown; *n* = 6–8 for CA1 recordings, and *n* = 7–9 for DG recordings. *, P < 0.05, using repeated measures ANOVA. (C) LTP at the SC-CA1 synapses was normal in Tg2576$^{+/-}$ and Vps35$^{+/m}$ mice but was defective in the 2-mo-old Tg2576$^{+/-}$;Vps35$^{+/m}$ mice. LTP was induced by one train of 100-Hz stimuli in the SCs. The upset shows representative traces of fEPSP recordings of responses before and 50 min after high frequency stimulation (HFS; arrow). (D) Quantitative analysis of data in C. The level of fEPSP potentiation was determined at a mean of 0–3 min and 50–60 min after high frequency stimulation. *n* = 5–7. (E) Severe LTP impairment at the SC-CA1 synapses in the 4-mo-old Tg2576$^{+/-}$;Vps35$^{+/m}$ mice. (F) Quantitative analysis of data in E. *n* = 5–7. (G) LTP at the DG was normal in Tg2576$^{+/-}$ and Vps35$^{+/m}$ mice but was defective in the 2–4-mo-old Tg2576$^{+/-}$;Vps35$^{+/m}$ mice. LTP was induced by a strong theta burst stimuli at the perforant pathway given at the time indicated by the arrow and recorded in the presence of 20 μM bicuculline (see Materials and methods). (H) Quantitative analysis of data in G. *n* = 8–11. (D, F, and H) *, P < 0.05; **, P < 0.01.

both AMPA and NMDA receptor-mediated mEPSCs in the double mutant CA1 neurons (Fig. 3, A, B, E, and F). This may be a result of a defective presynaptic glutamate release or reduction of the number of synapses. To further examine whether this is a result of a presynaptic defect, paired-pulse facilitation was measured. The ratio of paired-pulse facilitation was not significantly different among the four groups of mice (Fig. 3 H), suggesting that the decreased frequencies of both currents in the double mutant CA1 neurons may be caused by a reduction of the number of postsynaptic glutamatergic neurons/synapses. Consistent with the results in mEPSCs recordings, both amplitudes of evoked AMPA receptor-mediated and NMDA receptor-mediated EPSCs were lower in CA1 neurons from the double mutant slices as compared with the other three groups (Fig. 3 G), confirming the deficits of the glutamatergic synaptic transmission at the SC-CA1 synapses of young adult Tg2576$^{+/-}$;Vps35$^{+/m}$ mice.

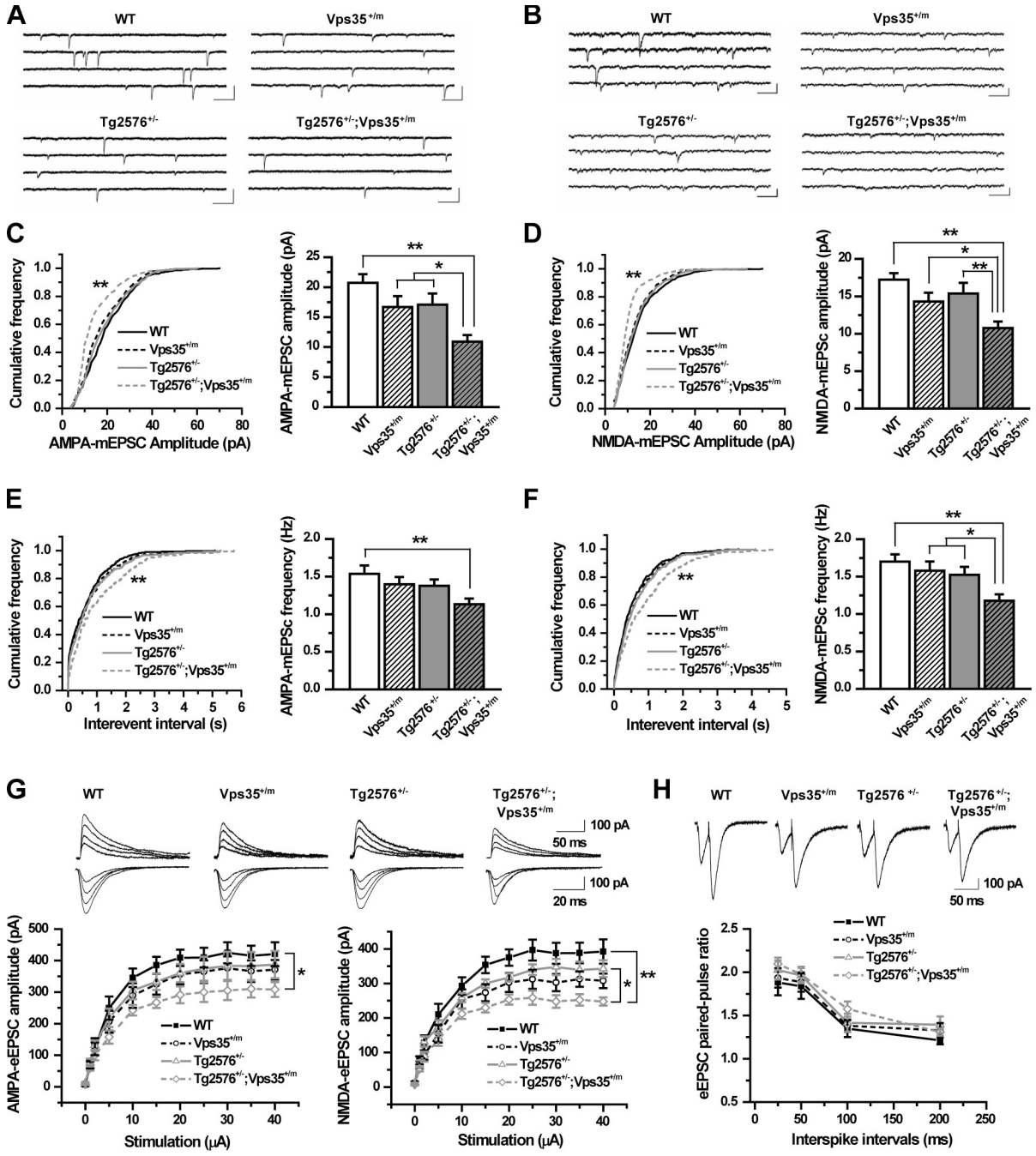

Figure 3. **Deficit in glutamatergic synaptic transmission in hippocampal CA1 pyramidal neurons of young adult Tg2576$^{+/-}$;Vps35$^{+/-}$ mice.** (A and B) Representative traces of AMPA (A) and NMDA (B) receptor-mediated mEPSCs. All mEPSCs were recorded at a holding potential of −65 mV. NMDA receptor-mediated mEPSCs were recorded in Mg^{2+}-free aCSF (see Materials and methods). Bars, 200 ms, 40 pA. (C and D) Cumulative distribution plots (left) and mean amplitude of AMPA receptor-mediated mEPSCs (C, right) and NMDA receptor-mediated mEPSCs (D, right). (E and F) Cumulative frequency plots of the interevent interval (left) and quantitative analysis of the frequency of AMPA receptor-mediated mEPSCs (E, right) and NMDA receptor-mediated mEPSCs (F, right). (G, bottom) Representative traces of eEPSCs (NMDA [right] and AMPA [left]) and quantitative analysis of evoked AMPA and NMDA receptor-mediated EPSC amplitude to stimulus intensity. AMPA and NMDA receptor-mediated EPSCs were recorded at a holding potential of −65 mV and +40 mV, respectively. (top) From left to right, the stimulus intensities for each trace were 2, 5, 10, and 30 μA (saturating stimulus). (H) Paired-pulse ratio analysis. Data were obtained from whole-cell recordings of CA1 pyramidal neurons from the four indicated groups of mice at the age of 2 mo old, including WT, Tg2576$^{+/-}$, Vps35$^{+/m}$, and Tg2576$^{+/-}$;Vps35$^{+/m}$ mice. (C–H) Data shown as mean ± SEM were analyzed by one-way ANOVA followed by Dunnett's test (for averaged mEPSC amplitude and frequency and paired-pulse ratio), Kolmogorov–Smirnov test (for mEPSC cumulative histograms), and repeated measures ANOVA (for eEPSC amplitude). *, $P < 0.05$; **, $P < 0.01$; $n = 9–16$.

Note that Tg2576$^{+/-}$ and Vps35$^{+/m}$ mutants also showed reductions of the amplitudes and frequencies of both AMPA and NMDA receptor-mediated mEPSCs and the amplitudes of both evoked AMPA and NMDA receptor-mediated EPSCs as compared with the WT control (Fig. 3, A–G), but these reductions were not statistically significant. We also examined GABAnergic neurotransmission in the four groups of mice by evaluating the miniature and evoked inhibitory postsynaptic currents (mIPSCs and

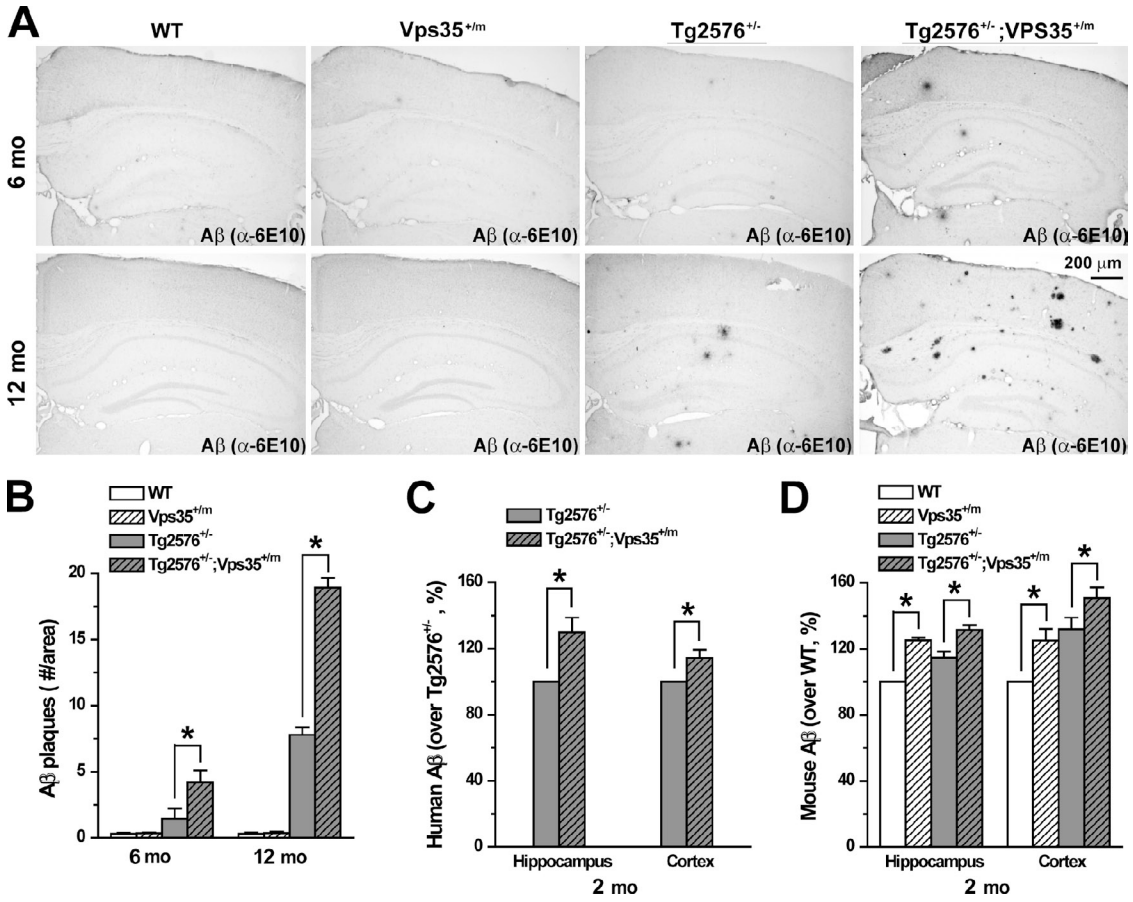

Figure 4. **Increase of Aβ deposits and $A\beta_{40}$ in the hippocampus and cortex by loss of VPS35 function.** (A and B) Increase of Aβ deposits in 6-mo or older $Tg2576^{+/-}$;$Vps35^{+/m}$ brain as compared with that of $Tg2576^{+/-}$ by immunohistochemical staining analysis using anti-6E10 antibody. Images are shown in A, and quantification data are presented in B (mean ± SEM; $n = 4$ for each of the genotypes). *, $P < 0.01$, with a significant difference from the control ($Tg2576^{+/-}$) by Student's *t* test. (C) Increase of human $A\beta_{40}$ levels in 2-mo-old $Tg2576^{+/-}$;$Vps35^{+/m}$ hippocampus and cortex as compared with that of $Tg2576^{+/-}$ mice. (D) Increase of mouse $A\beta_{40}$ levels in 2-mo-old hippocampus and cortex of $Vps35^{+/m}$ mice (compared with WT) and $Tg2576^{+/-}$;$Vps35^{+/m}$ mice (compared with $Tg2576^{+/-}$). (C and D) Hippocampus and cortex from WT and indicated mutant mice were homogenized with guanidine HCl extraction buffer, and the homogenates were analyzed by ELISAs for human (C) and mouse (D) $A\beta_{1-40}$. Data, shown as mean ± SEM, were analyzed by Student's *t* test. *, $P < 0.01$. $n = 4$ for each of the genotypes.

eIPSCs, respectively). Neither the frequency nor the amplitude of mIPSCs or eIPSCs was altered in the double mutant hippocampus (Fig. S2). Thus, these results demonstrate a decrease of glutamatergic, but not GABAnergic, neurotransmission, likely at the postsynaptic sites of the young adult double mutant hippocampus.

Increase of Aβ deposits and $A\beta_{40/42}$ in mouse hippocampus and cerebral cortex by loss of Vps35 function

The reduced glutamatergic neurotransmission corroborates with previous studies and may be caused by Aβ-induced neurotoxicity (Nimmrich et al., 2008; Selkoe, 2008). To determine whether Aβ production was increased in the $Vps35^{+/m}$;$Tg2576^{+/-}$ brain, we first examined for Aβ deposition by immunohistochemical staining. Aβ deposits or plaques were undetectable in brain sections of $Vps35^{+/m}$;$Tg2576^{+/-}$ mice or the other three genotypes at the age of 2–4 mo old (unpublished data). No Aβ deposit was observed in brain samples of WT or $Vps35^{+/m}$ mice as old as 12 mo (Fig. 4, A and B). Aβ deposits were rare in 6-mo-old $Tg2576^{+/-}$ brain but increased in number and size in 12-mo-old samples (Fig. 4, A and B), which is in agreement with a previous study (Hsiao et al., 1996). Interestingly, there are more, larger Aβ plaques in both 6- and 12-mo-old $Tg2576^{+/-}$;$Vps35^{+/m}$ brains in comparison with those in Tg2576 brain samples at respective ages (Fig. 4, A and B). These results demonstrate that Aβ deposits occurred in higher frequency and in younger $Vps35^{+/m}$;$Tg2576^{+/-}$ mice than that in Tg2576 mice.

To investigate mechanisms of how Aβ deposits were increased when VPS35 levels were reduced, we measured $A\beta_{40}$ levels in hippocampus and cerebral cortex. Tg2576 mice express the Swedish mutant form of human APP_{695} (Hsiao et al., 1996; Chapman et al., 1999; Rockenstein et al., 2007). ELISA analysis of human $A\beta_{40}$ detected Aβ in homogenates of hippocampus and cortex from Tg2576 mice, which is in agreement with previous studies (Hsiao et al., 1996; Chapman et al., 1999; Rockenstein et al., 2007). No human $A\beta_{40}$ was detected in WT or $Vps35^{+/m}$ mice (unpublished data). Remarkably, $A\beta_{40}$ levels were significantly higher in 2-mo-old $Tg2576^{+/-}$;$Vps35^{+/m}$ hippocampus and cerebral cortex as compared with Tg2576 littermate controls (by 30 and 15%, respectively; Fig. 4 C). A similar increase was also detected in 4–6-mo-old mice (unpublished data). These results indicated that $A\beta_{40}$ production is enhanced

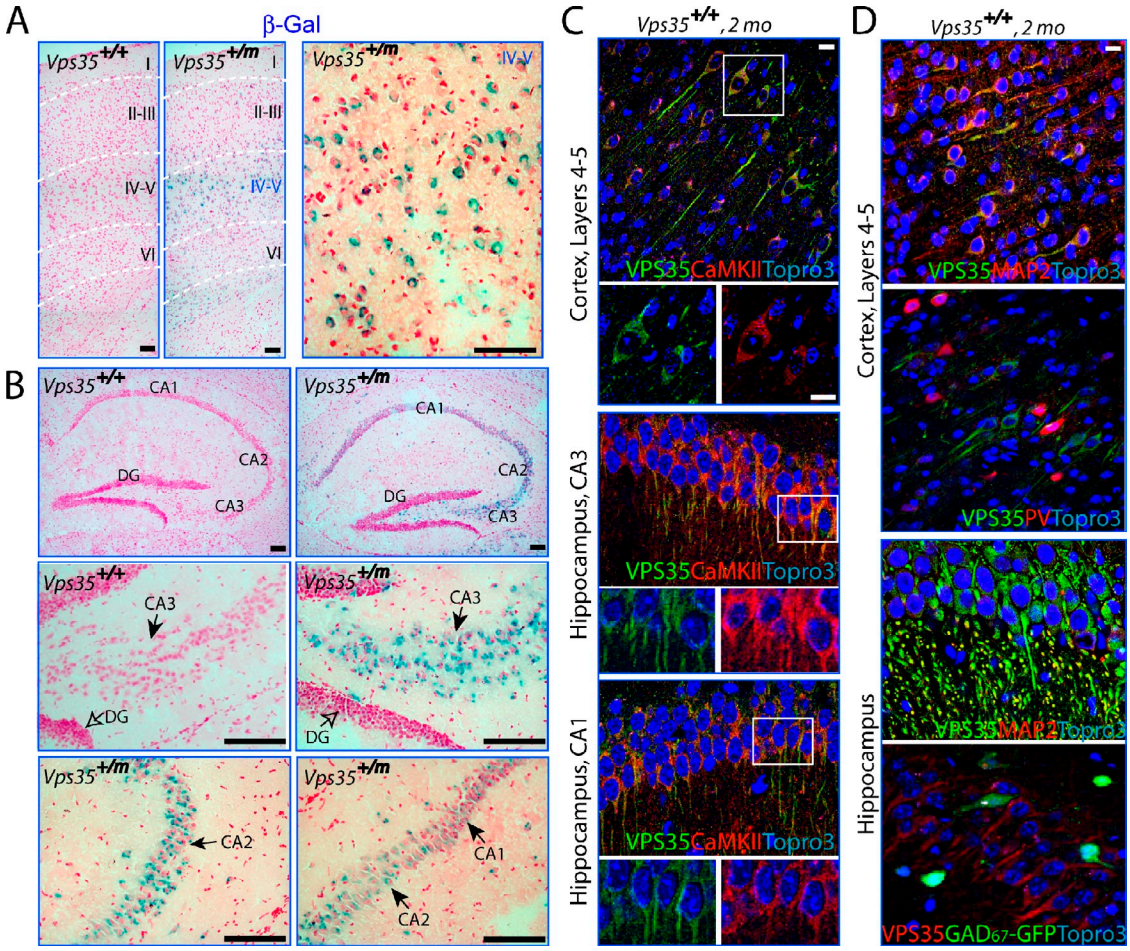

Figure 5. **VPS35 expression in pyramidal neurons of hippocampus and cortex.** (A and B) Detection of enzymatic LacZ activity in 2-mo-old WT ($Vps35^{+/+}$) and $Vps35^{+/m}$ cortex (A) and hippocampus (B). LacZ activity was only detected in $Vps35^{+/m}$ but not WT and was largely expressed in layer IV–V cortical neurons and CA1–3 hippocampus. Layers I–VI in cortex and DG and CA1–3 in hippocampus are indicated. Bars, 200 µm. (C and D) Immunofluorescence staining analysis of VPS35 protein distribution in pyramidal neurons of cortex and hippocampus from adult mouse brain. Confocal images of coimmunostaining analysis of VPS35 with CaMKII (C) and MAP2, parvalbumin (PV), and GAD67-GFP (D) are shown with their respective enlarged images of the boxed regions (C). Bars, 20 µm.

when VPS35 levels were reduced, suggesting that VPS35 negatively regulates $A\beta_{40}$ production. To test this hypothesis further, we examine the effect of Vps35 mutation on $A\beta_{40}$ production from endogenous APP on WT and Tg2576 background. Indeed, ELISA analyses of mouse $A\beta_{40}$ revealed an increase in the hippocampus and cerebral cortex of 2-mo-old $Vps35^{+/m}$ compared with WT (Fig. 4 D). Moreover, mouse $A\beta_{40}$ was also higher in the 2-mo-old $Tg2576^{+/-}$;$Vps35^{+/m}$ hippocampus and cerebral cortex than that of Tg2576 samples (Fig. 4 D). Elevated mouse $A\beta_{40}$ level was also detected in the hippocampus and cortex of 4–6-mo-old $Vps35^{+/m}$ mice (compared with the WT controls) and $Tg2576^{+/-}$;$Vps35^{+/m}$ mutant mice (compared with the $Tg2576^{+/-}$ mice; unpublished data). These results corroborate that VPS35 negatively regulates $A\beta_{40}$ production. In addition to $A\beta_{40}$, levels of human and mouse $A\beta_{42}$ were also increased by $Vps35^{+/m}$ mutation (Fig. S3 A and not depicted). However, the ratio of $A\beta_{40}$/$A\beta_{42}$ was not changed (Fig. S3 B), implicating that changes in VPS35 levels may not modulate the specificity of the γ-secretase cleavage of APP. Together, these data suggest that VPS35 negatively regulates Aβ production and support the view that increased Aβ levels may be a key detrimental factor for the cognitive and LTP deficits associated with the AD mice.

Expression of VPS35 in hippocampal and layer IV–V cortical pyramidal neurons and interaction of VPS35 with BACE1

We further determined in what cells VPS35 is expressed in the brain by taking advantage of the $Vps35^{+/m}$ mice. In these mice, the LacZ gene was knocked in in the intron of the Vps35 gene (Fig. S1 A); thus, LacZ expression is controlled by the promoter of the Vps35 gene. The β-gal activity was detectable in many layers or regions of the cortex and the hippocampus in neonatal mice but became restricted to layers IV–V in the cortex and CA2–3 regions of the hippocampus in adult mice (Fig. 5, A and B; and Fig. S4). The morphology of these neurons appeared to be excitatory pyramidal neurons. To determine whether this is the case, we costained the brain section with antibodies against VPS35 and CaMKII, a marker for pyramidal neurons. Indeed, VPS35 was codistributed with CaMKII in the soma and processes of neurons in the cortex and hippocampus (Fig. 5 C).

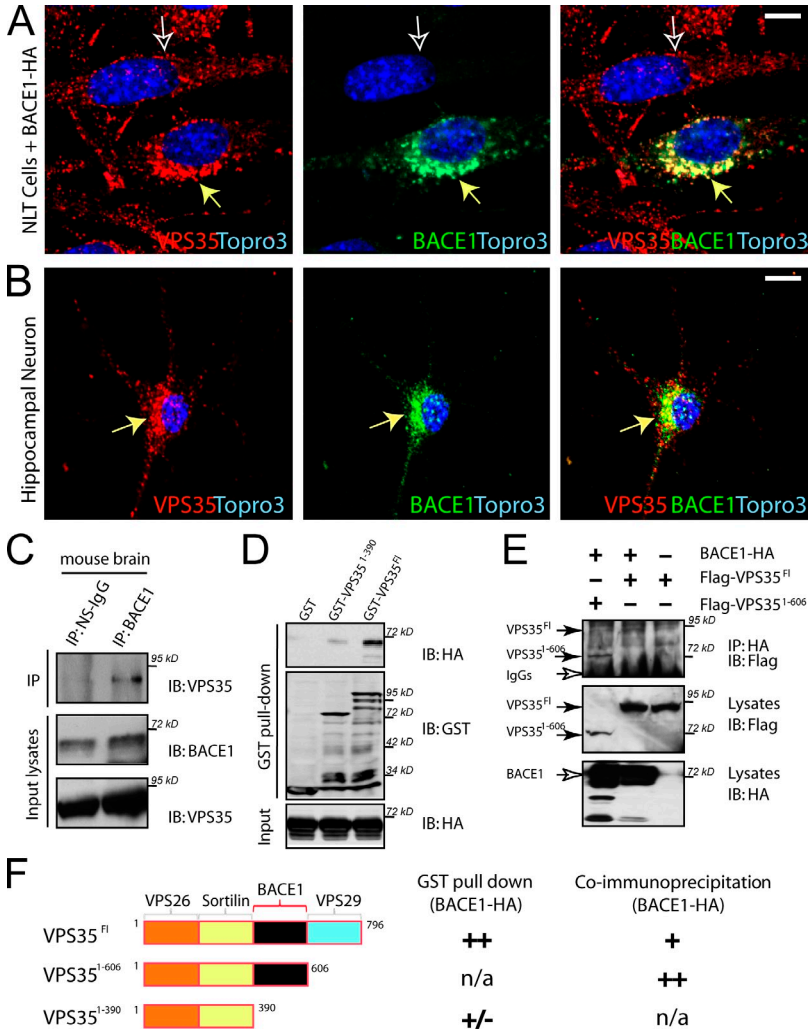

Figure 6. **VPS35–BACE1 interaction in vitro, in culture, and in mouse brain.** (A) Coimmunostaining analysis of exogenous BACE1 with endogenous Vps35 in NLT cells transfected with BACE1-HA. Closed arrows indicate their colocalization, and open arrows indicate BACE1-HA–negative cells. (B) Coimmunostaining analysis of endogenous BACE1 with Vps35 in primary cultured mouse cortical neurons (DIV3). Arrows indicate their colocalization. (A and B) Bars, 20 µm. (C) Coimmunoprecipitation (IP) analysis of VPS35–BACE1 protein complexes in homogenates of mouse brain. IB, immunoblotted; NS, nonspecific. (D) In vitro VPS35–BACE1 interaction revealed by GST pull-down assay. HEK293 cells expressing BACE1-HA were lysed, and resulting lysates were incubated with indicated GST fusion proteins (5 µg) immobilized on beads. Bound proteins were probed with anti-HA and -GST antibodies. (E) Coimmunoprecipitation analysis of VPS35–BACE1 protein complexes in lysates of HEK293 cells expressing the indicated plasmids. HEK293 cell lysates were incubated with anti-HA antibodies to immunoprecipitate BACE1 complexes, which were resolved on SDS-PAGE and immunoblotted with antibodies against Flag. BACE1 and VPS35 in lysates were revealed by immunoblotting with anti-HA and -Flag antibodies, respectively. (F) Illustration of VPS35 structure, its binding partners, and mutant VPS35 proteins and a summary of the data for VPS35–BACE1 interaction. n/a, not analyzed.

In contrast, the levels of VPS35 were low in interneurons, i.e., neurons labeled by parvalbumin in WT mice or GFP in GAD_{67}-GFP mice (Fig. 5, C and D). Subcellularly, VPS35 appeared to be enriched in dendrites that were labeled by MAP2, a dendritic marker in both the cortex and the CA1–3 regions of the hippocampus (Fig. 5 D).

$A\beta_{40/42}$ production requires BACE1. Thus, we determined whether VPS35 associates with BACE1 in neurons by coimmunostaining analysis. BACE1 and VPS35 were colocalized largely at perinuclear compartments in NLT cells, a cell line derived from GnRH neurons, and in mouse cortical neurons (Fig. 6, A and B). These results implicate a potential interaction between VPS35 and BACE1 in neurons. We further tested this view by coimmunoprecipitation analyses of mouse brain lysates, in which VPS35 was detected in BACE1-immunoprecipitated complexes (Fig. 6 C). We then mapped the interaction domain by in vitro GST pull-down assay and coimmunoprecipitation analysis of lysates from HEK293 cells expressing BACE1 and mutant VPS35. BACE1 displayed seemingly greater binding affinity for full-length VPS35 ($VPS35^{Fl}$) as compared with that of $VPS35^{1–390}$ in in vitro GST pull-down assays (Fig. 6, D and F). In coimmunoprecipitation analysis, however, $VPS35^{1–606}$ showed stronger association than that of the $VPS35^{Fl}$ (Fig. 6, E and F). These results support an interaction between VPS35 and BACE1 in vitro and in vivo and reveal a BACE1-binding site in VPS35 (the amino acids of 390–606; Fig. 6 F).

Increase of BACE1 in endosomal compartments in Vps35-deficient NLT cells and neurons

To investigate the potential function of VPS35–BACE1 interaction, we examined whether BACE1 subcellular distribution is regulated by VPS35. To this end, we generated small hairpin RNAs (shRNAs) and microRNAs (miRNAs) to suppress VPS35 expression. Transfection of shRNA-Vps35 or miRNA-Vps35, but not control (a scrambled miRNA), inhibited expression of cotransfected Flag-Vps35 in HEK293 cells (Fig. S5 A) and endogenous VPS35 in NLT cells (Fig. S5 B). HA-tagged BACE1 was present in perinuclear vesicles, close to Golgi apparatus, in control NLT cells (Fig. 7 A). In cells whose VPS35 expression was suppressed, BACE1 punctae were enlarged in size and no longer confined to the Golgi apparatus (Fig. 7 A). Instead, BACE1 became colocalized with LAMP1, a marker of late endosomes/lysosomes (Fig. 7, A and C), suggesting that VSP35 is critical for BACE1 to be localized in the Golgi apparatus, and, when VPS35 levels were lower, BACE1 is relocated. To further

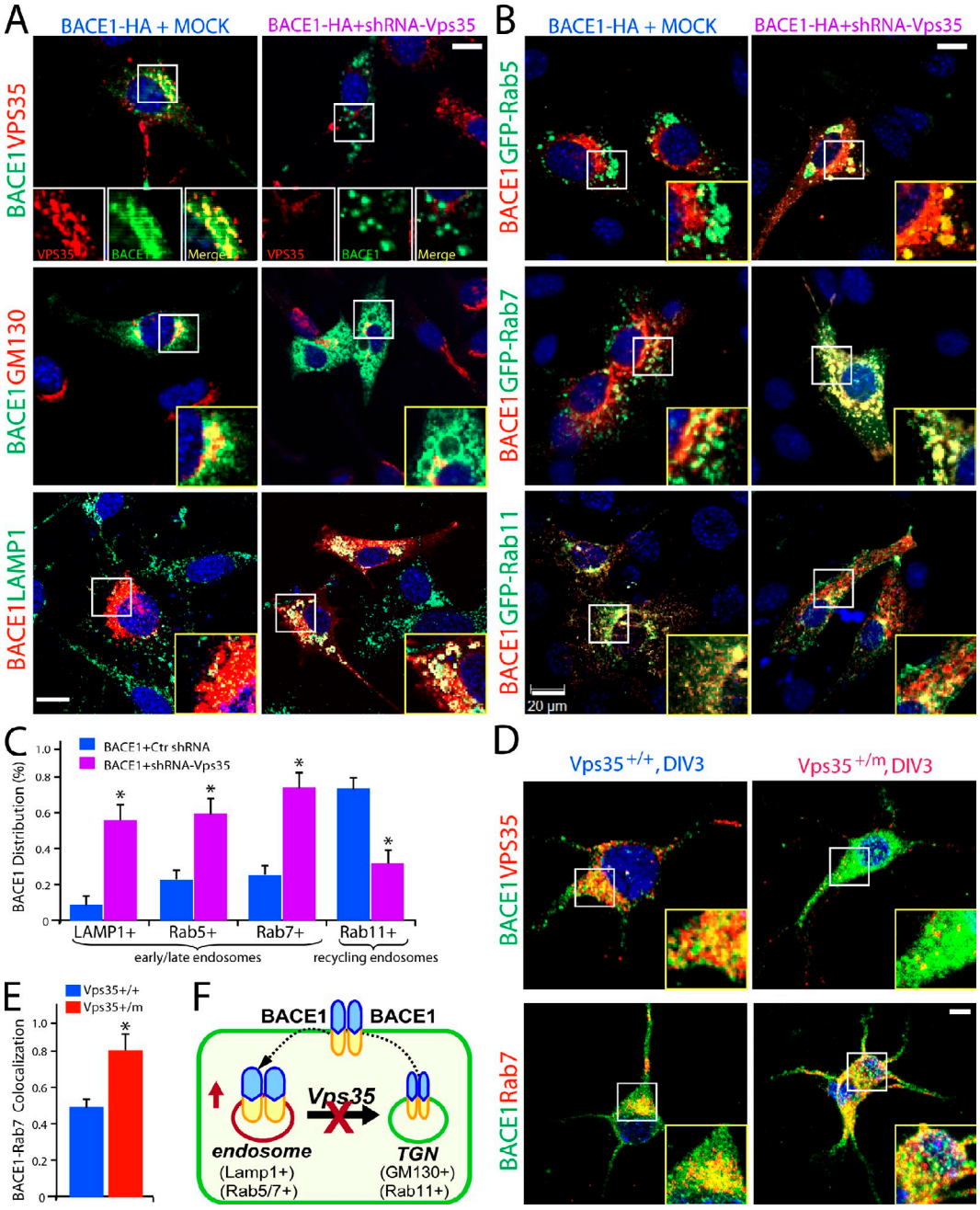

Figure 7. **Increase of BACE1 localization in endosomal compartments in NLT cells suppressing Vps35 expression and in Vps35$^{+/-}$ neurons.** (A) Co-immunostaining analysis of exogenous BACE1 with endogenous Vps35, GM130, and LAMP1 in NLT cells transfected with BACE1-HA with control or shRNA-Vps35. MOCK indicates control shRNA. (B) Coimmunostaining analysis of BACE1 with GFP-Rab5/7/11 in NLT cells coexpressing BACE1-HA and GFP-Rab5/7/11 with control or shRNA-Vps35. (A and B) Amplified images were included (indicated in the insets). (C) Quantification analysis of data from A and B using ImageJ. The colocalization index of BACE1 with the indicated markers (LAMP1 and Rab-5/7/11) was determined by the measurement of overlapped signal (yellow fluorescence) over total BACE1 signal. Data are shown as mean ± SEM (n = 5). *, $P < 0.01$ compared with control shRNA (Ctr shRNA) cells. (D) Coimmunostaining analysis of endogenous BACE1 with Rab7 in primary cortical neurons from WT and Vps35$^{+/m}$ mouse (E18 and DIV3). Amplified images are indicated in the insets. (E) Quantification analysis of data from D using ImageJ. The colocalization index of BACE1 with Rab7 was determined by the measurement of overlapped signal (yellow fluorescence) over total BACE1 signal. Data are shown as mean ± SEM (n = 5). *, $P < 0.01$ compared with WT neurons. (F) Illustration of the working model for Vps35 in BACE1 endosomal-to-Golgi retrieval. Bars, 20 μm.

study this phenomenon, we coexpressed various markers for early, late, and recycling endosomes (GFP-Rab5, Rab7, and Rab11, respectively). As shown in Fig. 7 (B and C), suppression of VPS35 expression increased BACE1 localization in both Rab5- and Rab7-positive endosomal compartments but reduced BACE1 in Rab11-labeled recycling endosomes. Similar effects were observed in NLT cells expressing miRNA-Vps35 (unpublished data). In agreement with this, BACE1-Rab7 colocalization was increased in neurons of Vps35$^{+/m}$ mice (Fig. 7, D and E). Collectively, these results demonstrate that VPS35 is required for the retrieval of BACE1 from endosomes to the Golgi apparatus in both NLT and hippocampal neurons (Fig. 7 F).

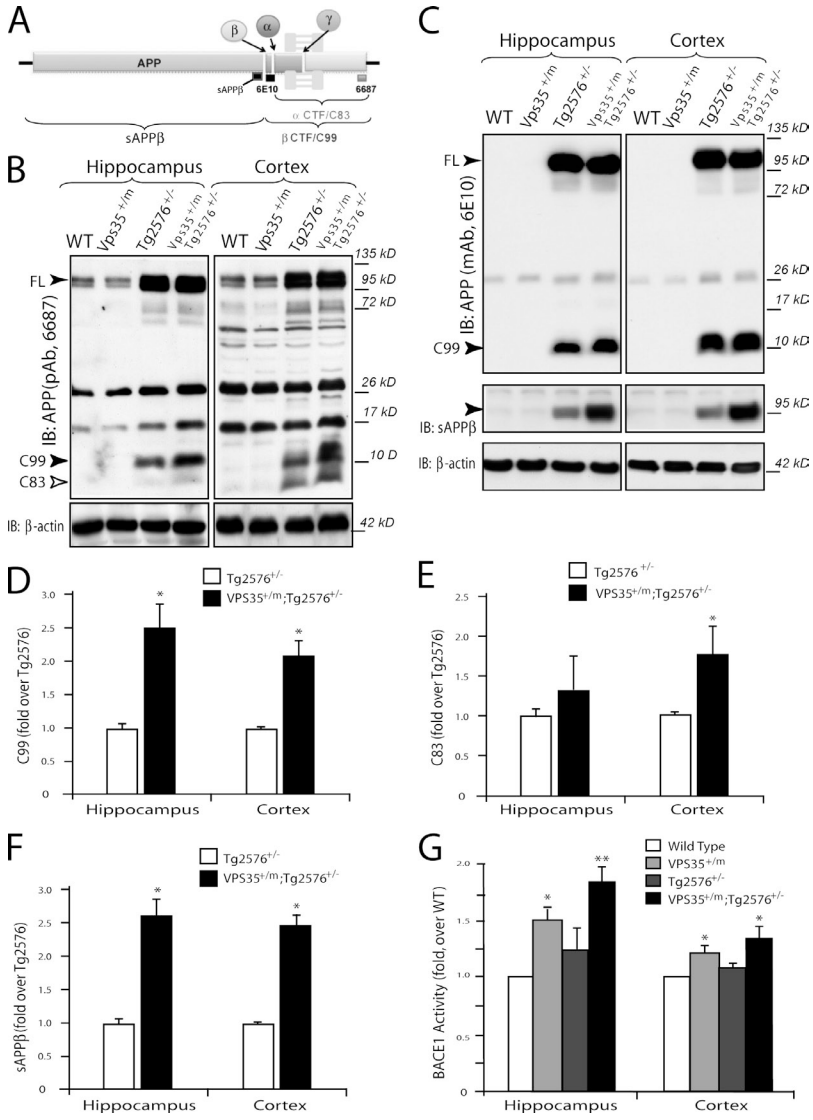

Figure 8. **Increase of BACE1-mediated cleavage of APP and BACE1 activity in young adult Tg2576$^{+/-}$;Vps35$^{+/m}$ hippocampus.** (A) Illustration of APP structure and its cleavage sites. The epitopes for the antibodies (sAPPβ, 6E10, and 6687) and the cleavage fragments (sAPPβ, βCTF/C99, and αCTF/C83) are indicated. (B and C) Western blot analysis of C99 and sAPPβ BACE1-mediated APP cleavage products using the indicated antibodies. Homogenates of cortex and hippocampus from 2-mo-old WT, Vps35$^{+/m}$, Tg2576$^{+/-}$, and Tg2576$^{+/-}$;Vps35$^{+/m}$ mice were subjected to Western blot analysis (16% Tricine SDS-PAGE; see Materials and methods). The full length (FL) of APP, the C99, sAPPβ, and C88 is indicated by arrows. APP$_{6687}$, but not 6E10, antibody also detected C83 (indicated by the open arrow), an α-secretase–mediated APP cleavage product. Equal amounts of homogenates (50 µg of protein) were loaded and revealed by immunoblot (IB) using anti–β-actin antibody. (D–F) Quantification analysis of C99 (D), C83 (E), and sAPPβ (F) cleavage products, in which three different experiments were quantified, and data were shown as mean ± SEM. *, $P < 0.05$, compared with Tg2576$^{+/-}$. (G) In vitro BACE1 activity measured by a BACE1 assay kit purchased from Abcam. The hippocampal and cortical homogenates from 2-mo-old WT and the indicated mutant mice were prepared for the in vitro BACE1 activity assay (see Materials and methods). The data were quantified from three to four different experiments and shown as mean ± SEM. *, $P < 0.01$ compared with WT control; **, $P < 0.01$ compared with Tg2576$^{+/-}$.

Increased BACE1-mediated cleavage of APP and BACE1 activity in VPS35 mutant mice

The aforementioned results demonstrate that VPS35 regulates BACE1 subcellular distribution. To determine whether these effects have any functional consequences, we measured BACE1 activity in Vps35$^{+/m}$ hippocampus and cortex. BACE1 activity was first determined by Western blot analysis of BACE1-mediated cleavage fragments (βCTF or C99 and sAPPβ) of APP (Fig. 8 A). Using 6E10, a monoclonal antibody that specifically recognizes the N-terminal 1–16 amino acid residues of human C99 and Aβ$_{40/42}$, βCTF or C99 was not detected in WT or Vps35$^{+/m}$ but was in Tg2576 hippocampus and cortex (Fig. 8 B). Interestingly, C99 levels were increased in Tg2576$^{+/-}$;Vps35$^{+/m}$ (Fig. 8, B–D), suggesting an increased activity of BACE1 when Vps35 was deficient. To test this hypothesis further, samples were analyzed by Western blots using a polyclonal antibody that specifically recognizes the sAPPβ and the 6687 polyclonal antibody that recognizes both C99 and C83 (an α-secretase cleavage product; Fig. 8 A). Again, levels of sAPPβ and C99 were increased in Tg2576$^{+/-}$;Vps35$^{+/m}$ hippocampus compared with Tg2576 alone (Fig. 8, B–F). However, C83 levels were not consistently altered by Vps35 mutation (Fig. 8, C and E), suggesting that Vps35 mutation had no or weak effect, if there is any, on α-secretase activity. Together, these results indicate that loss of Vps35 promotes BACE1-mediated cleavage of APP or APPswe, thereby increasing Aβ production.

We then measured the BACE1 activity directly by an in vitro assay in both hippocampus and cortex from the four different groups at the age of 2 mo old (Fig. 8 G). Approximately 25 and 10% increases of BACE1 activity were found in Tg2576$^{+/-}$ hippocampus and cortex, respectively (compared with the WT control; Fig. 8 G), which is in line with previous studies (Fukumoto et al., 2002; Yang et al., 2003). Interestingly, Vps35$^{+/m}$ hippocampus and cortex exhibited significant increases of BACE1 activity by ∼50 and 20%, respectively, as compared with that of WT controls (Fig. 8 G). The double mutant showed a further increase of BACE1 activity in both hippocampus and cortex as compared with the single mutant mice (Fig. 8 G). Note that the increase of BACE1 activity in the mutant hippocampus was more dramatic as compared with

that in the cortex (Fig. 8 G). Thus, these results support the notion that loss of VPS35 function leads to an increase of BACE1 activity and thus Aβ production.

Discussion

VPS35, a major component in the cargo recognition complex of retromer, plays an important role in endosome-to-Golgi retrieval of multiple membrane proteins. Although retromer is implicated in the pathogenesis of late-onset AD, the function of VPS35 in AD pathology and the underlying molecular mechanisms remain largely unclear. In this study, we showed that Vps35 regulates BACE1 cellular trafficking, and loss of Vps35 function leads to an increase of BACE1 activity and Aβ levels (Figs. 4–8). Tg2576 mice with reduced VPS35 expression exhibit an earlier onset of AD-like phenotypes, including cognitive memory deficits, reduced LTP, and decreased glutamatergic neurotransmission in 2-mo-old mice (Figs. 1–3). We also demonstrated that knocking down VPS35 expression in cultured cells increased BACE1 localization to the endosomal compartments where the BACE1 cleavage of APP is favored, providing a mechanism underlying VPS35/retromer regulation of BACE1 activation (Fig. 7 F). Moreover, we demonstrated that VPS35 is highly expressed in pyramidal neurons in young adult CA1–3 hippocampus, interacts with BACE1, and regulates BACE1 distribution. Collectively, our work provides strong evidence for VPS35 to be a crucial component in BACE1 trafficking, APP metabolism, and hippocampal neuronal synaptic function and establishes a novel mouse model in which impaired retromer function leads to altered BACE1 activation and Aβ production, thus facilitating AD disease progression in an age-dependent manner.

Many animal models have been developed for the study of pathological features of AD, including Tg2576, a transgenic line expressing Swedish mutant APP. Tg2576 mice normally develop AD-like phenotypes, including cognitive deficits and Aβ deposits, at the age of at least 10 mo or older (Chapman et al., 1999; Middei et al., 2006; Bizon et al., 2007). Remarkably, the double mutant mice ($Vps35^{+/m}$;$Tg2576^{+/-}$) develop AD-like phenotypes at the age of 2/3 mo old, featured with cognitive memory deficit, synaptic plasticity (LTP) impairments, decrease of glutamatergic transmissions, and increase of Aβ levels (Figs. 1–4). These observations demonstrate that VPS35 plays an important role in the control of the early onset of AD neuropathology, contributing to the growing body of evidence for the retromer-sorting pathway in the pathogenesis of AD.

The double mutant mice ($Vps35^{+/m}$;$Tg2576^{+/-}$) display impairments in NMDA and AMPA receptor-mediated synaptic transmission and synaptic plasticity (LTP) but not GABAergic transmission. These defects may be caused by a loss of excitatory synapses and/or a decrease of glutamatergic synaptic activity, which contribute to the progressive cognitive decline in the mutant mice. Our data corroborate with the view that the decreased NMDA and AMPA currents may be induced by the increase of soluble Aβ oligomers, but not Aβ deposits, in the double mutant brain (Nimmrich et al., 2008; Selkoe, 2008), as these deficits occur as early as 2 mo old, whereas Aβ deposition is detectable at the age of 6 mo and older. On the other hand, it cannot be excluded in an Aβ-independent mechanism that may also contribute to the loss of synapses and synaptic activity in the double mutant hippocampus. Note that the hippocampus of $Vps35^{+/m}$ in the WT background also exhibits an increase of Aβ levels, a decrease of synaptic activity (both NMDA and AMPA currents), and a loss of synapses (decrease of frequency of mEPSCs) but without obvious defects on cognitive learning and memory or LTP (Figs. 1–4). These observations suggest that it may need to reach a threshold level of Aβ (as does the double mutant but not $Vps35^{+/m}$) or an Aβ-independent factor to induce the loss of synaptic plasticity and cognitive deficit. It is possible that loss of Vps35 function may predispose neurons to a greater Aβ toxicity and may facilitate disease progression in an age-dependent manner.

Genetic, biochemical, animal, and human studies have all pointed to Aβ peptide to be a major culprit in AD pathogenesis (Tanzi and Bertram, 2005; Selkoe, 2008). Identification of mutations in APP and presenilins in the early-onset AD provides a strong genetic support for the amyloid hypothesis (Hardy and Selkoe, 2002). Many risky factors associated with the late-onset AD also affect APP metabolism and increase Aβ production, which include ApoE4 and SorL1 (Rogaeva et al., 2007; Willnow et al., 2010). Interestingly, SorL1 is a Vps10 family member in the retromer complex that interacts with APP and VPS35, and the interaction of SorL1 with VPS35 is necessary for SorL1 to control APP metabolism (Lane et al., 2010). Our results, in line with these observations, support the view for the dysfunction of VPS35-containing retromer as a risk factor for AD. This view is also supported by the observation that VPS35 is decreased in the postmortem hippocampus of AD patients (Small et al., 2005). Of interest to note is that loss of function of SorCS1, a SorL1 family protein and a risk factor for type 2 diabetes, also leads to an increase of Aβ and a decrease of VPS35 levels (Lane et al., 2010), raising a possibility for the involvement of Vps35 retromer in regulating insulin sensitivity in addition to APP metabolism. Also of interest to note is that mutation in Vps35 gene has recently been identified in patients of late-onset Parkinson's disease (PD; Vilariño-Güell et al., 2011; Zimprich et al., 2011), indicating the involvement of Vps35 in the pathogenesis of PD. Thus, these observations together with our results support the view for the impairment of Vps35 retromer as a general risky factor for a growing number of chronic degenerative disorders, including AD and PD.

How does retromer regulate Aβ production? Our data suggest that BACE1 activation in the $Vps35^{+/m}$ hippocampus may be essential for this event. VPS35 is codistributed with BACE1 in hippocampus (not depicted) and in cultured cells (Fig. 6). Loss of VPS35 function in mouse hippocampus increases BACE1 activity (Fig. 8). Depletion of Vps35 expression in culture increases BACE1 localization to the endosomal compartments (Fig. 7), an acidic environment favoring BACE1 activation. Although our experiments have pointed to the importance of endosomal BACE1 cleavage of APP, it remains to be further investigated whether the activity of Golgi/endosome-associated BACE1 is altered by loss of Vps35 function, in which subcellularly Aβ is produced in Vps35-deficient neurons, and whether APP and APPswe protein trafficking is differentially regulated

by VPS35. It is likely that, in addition to BACE1 activation, altered APP metabolism also contributes to the elevated Aβ levels in Vps35-deficient neurons. The observation that SorL1 interaction with VPS35 is required for SorL1 to control APP metabolism (Willnow et al., 2010) supports this view. The increased Aβ levels in both $Vps35^{+/m}$ and $Vps35^{+/m}$;Tg2576 mutant mice (Fig. 4, C and D) suggest a role for VPS35 not only in regulating WT APP, but also APPswe, metabolism. However, mechanisms underlying VPS35 regulation of APPswe and WT APP may be different, as it is reported that APPswe exhibits a much higher affinity to BACE1 as compared with the WT APP, and APPswe may be cleaved by BACE1 at the TGN, whereas WT APP may be cleaved at the endosome compartments (Haass et al., 1995; Selkoe et al., 1996; Thinakaran and Koo, 2008). Collectively, the data presented in this manuscript suggest an important function of VPS35 in suppression of BACE1 activation and Aβ production, thus preventing AD-associated memory cognitive deficits and impairment of glutamatergic synaptic activity.

Materials and methods

Reagents and animals

Rabbit polyclonal anti-VPS35 antibody was generated using the antigen of GST-VPS35D1 fusion protein, as previously described (Small et al., 2005). Rabbit polyclonal anti-APP6678 (Invitrogen) and anti-BACE1 (Millipore) antibodies and monoclonal anti-APP (6E10; Covance), BACE1 (Millipore), CaMKII (Clone 6G9; Millipore), parvalbumin (PV235; Swant, Inc.), and MAP2 (Millipore) antibodies were used. Other chemicals and reagents used in this study were of analytical grade.

Vps35 mutant mice were generated by injection of mutant ES cells obtained from Bay Genomics. In brief, ES cells that contain the Vps35 gene disrupted by gene trapping using the pGT1TMpt vector (Fig. S1 A) were obtained from Bay Genomics. ES cell clones were transferred into mouse blastocysts. Chimeras generated from ES cells were crossed to C57/BL6 mice for more than six generations, and the resulting heterozygous animals were crossed to Tg2576 mice (purchased from Taconic) to produce four different genotyped mice (WT, $Tg2576^{+/-}$, $Vps35^{+/m}$, and $Tg2576^{+/-}$;$Vps35^{+/m}$). Mice were maintained on a standard rodent diet (Teklad S-2335; Harlan Laboratories, Inc.). Control littermates (WT, $Vps35^{+/m}$, and $Tg2576^{+/-}$) and $Tg2576^{+/-}$;$Vps35^{+/m}$ were processed in parallel for each experiment. Tg2576 and Vps35 mutations were confirmed by genotyping using PCR (Fig. S1 B). All experimental procedures were approved by the Animal Subjects Committee at the Georgia Health Sciences University, according to National Institutes of Health guidelines.

Expression vectors

The cDNAs encoding Vps35 were amplified by PCR and subcloned into mammalian expression vectors downstream of a signal peptide and a Flag epitope tag (MDYKDDDDKGP) and under control of the cytomegalovirus promoter (Ren et al., 2004; Xie et al., 2005). The shRNA-Vps35 expression vector was generated by the pSuper vector system, and the miRNA-Vps35 expression vector was generated by the BLOCK-iT Lentiviral miR RNAi expression system (Invitrogen) according to the manufacturer's instructions (Zhu et al., 2007). The plasmid encoding BACE1-HA was generated by insertion of the HA tag to the C terminus of the human BACE1 in the pcDNA3 vector, as previously described (Hu et al., 2010). The plasmids encoding GFP-Rab5, GFP-Rab7, and GFP-Rab11 were obtained from Addgene and deposited by R. Pagano (Mayo Clinic, Rochester, MN). The authenticity of all constructs was verified by DNA sequencing.

Behavior tests

Behavioral analysis was performed with 1–2-, 3-, and 6-mo old mice by investigators unaware of their genotype. The Morris water maze testing was performed as previously described (Morris, 1991). The maze consisted of a pool (120 cm in diameter) filled with water (22 ± 1°C) made opaque white with bright white food color (1498A; AmeriColor), and the pool was located in a room surrounded by distinct extra maze cues. Before hidden-platform training, mice were given one pretraining trial in which no platform was placed in the pool, and mice had to swim in the pool for 60 s. Mice that had less motivation for swimming were excluded from the experiment. The day after pretraining, mice were trained in the circular water maze. For hidden-platform training, the escape platform (10 cm in diameter) was submerged 1.0 cm beneath the water surface. The platform location remained the same throughout hidden-platform training, but the drop location varied semirandomly between trials. Mice received one training session for a consecutive 5 d. Each session consisted of four trials with a 1-min intertrial interval. The maximum time allowed per trial in this task was 120 s. If a mouse did not find the platform, it was gently guided to it and allowed to sit on it for 30 s before being removed to its retaining cage. The mean latency and distance moved were calculated for each mouse by averaging the latency and distance across all four trials. For probe trials, the platform was removed, and mice were allowed to swim for 60 s before they were removed. The drop location for probe trials was 180° from where the platform was located during hidden-platform training. The swimming behavior was monitored by camera (WV-BP334; Panasonic), and images and swimming paths were stored in a computer and analyzed automatically by using EthoVision software (version 7.0; Noldus Information Technology).

The spontaneous locomotor activity in an open field was measured as previously described (Wen et al., 2010). The mice were transferred to the testing room and acclimated for at least 3 d before testing. Mice were then placed in an open field chamber (27.9 × 27.9 cm) that uses a series of horizontally mounted photobeams to monitor animal movements (Med Associates Inc) for 10 min. Ambulatory activity was measured as total horizontal photobeam breaks (horizontal activity). The apparatus was cleaned with 70% alcohol between testing of each mouse. Total movements (ambulations) in the outer periphery and center of the open field were recorded for further data analysis.

Electrophysiological recording

Brain slices were prepared using standard procedures (Wen et al., 2010). In brief, transverse hippocampal slices (0.40 mm) were prepared from WT and mutant littermates using a Vibroslice (VT 1000S; Leica) in an ice-cold solution containing 64 mM NaCl, 2.5 mM KCl, 1.25 mM NaH_2PO_4, 10 mM $MgSO_4$, 0.5 mM $CaCl_2$, 26 mM $NaHCO_3$, 10 mM glucose, and 120 mM sucrose. Slices were allowed to recover for 30 min at 34°C and then at room temperature (25 ± 1°C) for an additional 2–8 h in artificial cerebrospinal fluid (aCSF) containing 126 mM NaCl, 2.5 mM KCl, 1.25 mM NaH_2PO_4, 2 mM $MgSO_4$, 2 mM $CaCl_2$, 26 mM $NaHCO_3$, and 10 mM glucose. Slices were transferred to the recording chamber and superfused with aCSF (2 ml/min) at 34°. All solutions were saturated with 95% O_2/5% CO_2 (volume/volume). fEPSPs were evoked in the CA1 stratum radiatum or in the stratum moleculare of the DG by stimulating the SCs/commissural pathway (for CA1) or the perforant pathway (for DG) with a two-concentrical bipolar stimulating electrode (25-mm pole separation; FHC, Inc) and were recorded in current-clamp by the Axon MultiClamp 700B amplifier (Molecular Devices) with aCSF-filled glass pipettes (2–5 MΩ). Test stimuli consisted of monophasic 100-µs pulses of constant currents (with intensity adjusted to produce 25% of the maximum response) at a frequency of 0.0167 Hz. The strength of synaptic transmission was determined by measuring the initial (10–60% rising phase) slope of fEPSPs. LTP in the CA1 area was induced by one train of 100-Hz stimuli with the same intensity of the test stimulus, and a cut was made between CA1 and CA3 in hippocampal slices to prevent the propagation of epileptiform activity. For LTP experiments in the DG, slices were incubated in 20 µM bicuculline to block $GABA_A$-mediated inhibition, and LTP was induced by the theta burst stimulation (six pulses at 250 Hz, with bursts delivered at a frequency of 5 Hz, and six trains of bursts delivered six times, with 20 s between trains).

For whole-cell patch-clamp recordings, stratum pyramidal of CA1 neurons were visualized using an infrared differential interference contrast microscope with a 40× water immersion lens (Axioskop 2 Fs Plus; Carl Zeiss) and an infrared-sensitive charge-coupled device camera. All experiments were conducted on neurons located within the cell-dense band CA1 region and bearing pyramidal-shaped cell bodies with single apical dendrites. Whole-cell patch-clamp recordings were performed using an amplifier (Axon Multiclamp 700B) and digitized by pClamp software (version 9.2; Molecular Devices). Both mEPSCs and mIPSCs were recorded at a holding potential of −65 mV. For mEPSC recording, glass pipettes were filled with the solution containing 120 mM K-gluconate, 20 mM KCl, 10 mM Hepes, 0.1 mM EGTA, 2 mM $MgCl_2$, 10 mM sodium phosphocreatine, 0.2 mM leupeptin, 4 mM Mg-ATP, and 0.3 mM Na-GTP, pH 7.3 (280 mOsm). K-gluconate in the pipette solution was substituted with 140 mM

KCl (final concentration) for mIPSC recording. NMDA receptor-mediated mEPSCs were recorded in a modified aCSF (0 mM $MgSO_4$, 5 mM KCl, and 1.6 mM $CaCl_2$). For evoked EPSC (eEPSC) and eIPSC recording, K-gluconate was substituted with 120 mM $CsCH_3SO_3$, and 5 mM lidocaine *N*-ethylchloride (QX-314) was added in the pipette. The resistance of pipettes was 3–5 MΩ. AMPA and NMDA receptor-mediated EPSCs were recorded at a holding potential of −65 mV and +40 mV, respectively; eIPSCs were recorded at a holding potential of −65 mV. 1 µM tetrodotoxin was included in the perfusion solution for mEPSC and mIPSC recording. For mEPSC and eEPSC recordings, 20 µM bicuculline was used to block $GABA_A$ receptor-mediated currents, and NMDA receptor-mediated eEPSCs were recorded in the presence of 20 µM 6-cyano-7-nitroquinoxaline-2,3-dione (CNQX). For mIPSC and eIPSC recording, 50 µM DL-2-amino-5-phosphonovaleric acid and 20 µM CNQX were supplemented to block NMDA and AMPA receptors, respectively. Stock solutions of all drugs were diluted to working concentrations in the extracellular solution immediately before use and applied by continuous superfusion. eEPSCs and eIPSCs were generated with a two-concentric bipolar stimulating electrode (FHC, Inc) positioned ∼200 µm from the neuron under recording. Single pulses of 0.1 ms were delivered at 0.1 Hz and synchronized using a Mater-8 stimulator (A.M.P.I.). Data were filtered at 2 kHz and sampled at 10 kHz. Neurons with a resting potential of at least −60 mV and resistance fluctuated within 15% of initial values (<20 MΩ) were analyzed. Mini events were analyzed with MiniAnalysis software (Synaptosoft, Inc.). The amplitude histograms were binned at 1 pA. Differences between cumulative histograms were evaluated using the Kolmogorov–Smirnov test.

Analysis of $A\beta_{40/42}$ levels and in vitro measurement of BACE1 activity

Mouse $A\beta_{40}$ (catalog no. KMB3481) and $A\beta_{42}$ (catalog no. KMB3441) and human $A\beta_{40}$ (catalog no. KHB3481) and $A\beta_{42}$ (catalog no. KHB3441) were detected using immunoassay (colorimetric) kits purchased from Invitrogen, as previously described (Johnson-Wood et al., 1997). In brief, cortex and hippocampal tissues for ELISAs were homogenized in 8 vol of ice-cold guanidine buffer (5.0 M guanidine HCl/50 mM Tris HCl, pH 8.0). The homogenates were further diluted (at 1:10) with ice-cold reaction buffer BSAT-DPBS (Dulbecco's PBS with 5% BSA and 0.03% Tween 20, supplemented with 1× protease inhibitor cocktail). The supernatants were collected after the centrifugation (16,000 *g* for 20 min at 4°C) of the homogenates and subjected to the Aβ ELISA analysis using the kits according to the manufacturer's instructions. The β-secretase activity (catalog no. ab65357) was also measured using a kit purchased from Abcam, according to the instructions.

Western blot analysis of APP cleavage products

APP cleavage products C83/C99 were determined by Western blot analysis as previously described (Zha et al., 2004). Specifically, samples (40 µg) were separated by 16% Tris-Tricine SDS-PAGE and electrophoretically transferred onto nitrocellulose membrane at 380 mA for 60 min. The blotted membrane was heated in boiling PBS for 5 min to enhance the signal. The blot was probed with the indicated APP antibodies (6E10 and 6687).

β-Gal detection, immunofluorescence staining, and confocal imaging analysis

Brain sections derived from adult mice (WT, heterozygotes, and $Tg2576^{+/-}$; $Vps35^{+/m}$) were fixed with 0.5% glutaraldehyde and incubated with X-gal solution (2 mM $MgCl_2$, 5 mM potassium ferricyanide, 5 mM potassium ferrocyanide, and 0.1% X-gal) in the dark at 37°C for 8 h, as previously described (Lee et al., 2010; Zhou et al., 2010). For immunohistochemical staining, age-matched littermates were perfused transcardially with 4% PFA in 0.1 M PBS, and brain tissues were postfixed at 4°C for 24 h. Paraffin sections (∼10 µm in thickness) were subjected to the immunohistochemical staining analysis of the Aβ plaques (by 6E10 antibody). The staining signal was revealed by reaction with an HRP system (DAB; Invitrogen). Transfected cells on the coverslips were fixed with 4% PFA and 4% sucrose at room temperature for 45 min, permeabilized in 0.15% Triton X-100 for 8 min, and then subjected to coimmunostaining analysis using indicated antibodies, as previously described (Zhu et al., 2007). Confocal images were obtained using an oil immersion 40 or 63× objective (LSM510; Carl Zeiss). For fluorescent quantification, morphometric measurements of images were performed using ImageJ software (National Institutes of Health).

Cell culture and transient transfection

NLT and HEK293 cells were maintained in DME supplemented with 10% FCS and 100 U/ml penicillin G and streptomycin (Invitrogen). Mouse cortical neuron cultures were prepared at a density of 25,000 cells per cm^2 on polyornithine-coated coverslips from cortical tissues of E18–19 mouse embryos, as previously described (Xie et al., 2005). Neurons were grown overnight in plating medium (5% FBS and 1× B27 supplemented with 100× L-glutamine in Neurobasal medium [Invitrogen]). Starting at day in vitro 2 (DIV2), cultures were maintained in conditioned medium with half-feed changes of neuronal feed (1× B27 in Neurobasal medium) every 3 d. For transfection, NLT cells were plated at a density of 10^6 cells per 10-cm culture dish and allowed to grow for 12 h before transfection using Lipofectamine. 36 h after transfection, cells were subjected to immunostaining analysis. The calcium phosphate method was used for transfection of HEK293 cells. 48 h after transfection, cells were lysed in modified radioimmunoprecipitation assay buffer (50 mM Tris-HCl, pH 7.4, 150 mM sodium chloride, 1% NP-40, 0.25% sodium deoxycholate, and proteinase inhibitors). Lysates and medium were subjected to immunoblotting analyses. Neurons were transfected with various constructs at either DIV4 or 7 using the calcium phosphate method followed by immunocytochemistry 96 h after transfection, as previously described (Zhu et al., 2007).

Statistical analysis

All data were expressed as mean ± SEM. All data were analyzed by one-way or repeated measures analysis of variance (ANOVA; SPSS16) followed by the least significant difference or Dunnett's test for post hoc comparisons or an independent sample *t* test unless otherwise specified. The significance level was set at $P < 0.05$.

Online supplemental material

Fig. S1 demonstrates the generation of $Vps35^{+/m}$ and $Tg2576^{+/-}$;$Vps35^{+/m}$ mutant mice. Fig. S2 depicts the normal inhibitory synaptic transmission in hippocampal CA1 pyramidal neurons of $Tg2576^{+/-}$;$Vps35^{+/m}$ mice. Fig. S3 shows an increase of $A\beta_{42}$ in young adult $Tg2576^{+/-}$;$Vps35^{+/m}$ hippocampus without a change of the ratio of $A\beta_{40}$ versus $A\beta_{42}$ in the mutant mice. Fig. S4 demonstrates an age-dependent reduction of Vps35 expression in CA1 and cortical neurons. Fig. S5 shows the suppression of Vps35 expression by both shRNA and miRNA-Vps35. Online supplemental material is available at http://www.jcb.org/cgi/content/full/jcb.201105109/DC1.

We thank Dr. Yi Xie for the initial isolation of mouse Vps35 clone, Ms. Sunnie Xiong for mouse maintenance and genotyping, and members of the Xiong and Mei laboratories for helpful discussions.

This study was supported in part by grants from the National Institutes of Health National Institute of Neurological Disorders and Stroke (to W.-C. Xiong and L. Mei). W-C. Xiong and L. Mei are coinventors on one patent application involving a Vps35 mutant mouse.

The authors have no other conflicting financial interests.

Submitted: 20 May 2011
Accepted: 21 October 2011

References

Arighi, C.N., L.M. Hartnell, R.C. Aguilar, C.R. Haft, and J.S. Bonifacino. 2004. Role of the mammalian retromer in sorting of the cation-independent mannose 6-phosphate receptor. *J. Cell Biol.* 165:123–133. http://dx.doi.org/10.1083/jcb.200312055

Ashe, K.H., and K.R. Zahs. 2010. Probing the biology of Alzheimer's disease in mice. *Neuron*. 66:631–645. http://dx.doi.org/10.1016/j.neuron.2010.04.031

Belenkaya, T.Y., Y. Wu, X. Tang, B. Zhou, L. Cheng, Y.V. Sharma, D. Yan, E.M. Selva, and X. Lin. 2008. The retromer complex influences Wnt secretion by recycling wntless from endosomes to the trans-Golgi network. *Dev. Cell*. 14:120–131. http://dx.doi.org/10.1016/j.devcel.2007.12.003

Bertram, L., and R.E. Tanzi. 2008. Thirty years of Alzheimer's disease genetics: The implications of systematic meta-analyses. *Nat. Rev. Neurosci.* 9:768–778. http://dx.doi.org/10.1038/nrn2494

Bizon, J., S. Prescott, and M.M. Nicolle. 2007. Intact spatial learning in adult Tg2576 mice. *Neurobiol. Aging*. 28:440–446. http://dx.doi.org/10.1016/j.neurobiolaging.2006.01.004

Bonifacino, J.S., and J.H. Hurley. 2008. Retromer. *Curr. Opin. Cell Biol.* 20:427–436. http://dx.doi.org/10.1016/j.ceb.2008.03.009

Canuel, M., S. Lefrancois, J. Zeng, and C.R. Morales. 2008. AP-1 and retromer play opposite roles in the trafficking of sortilin between the Golgi apparatus and the lysosomes. *Biochem. Biophys. Res. Commun.* 366:724–730. http://dx.doi.org/10.1016/j.bbrc.2007.12.015

Chapman, P.F., G.L. White, M.W. Jones, D. Cooper-Blacketer, V.J. Marshall, M. Irizarry, L. Younkin, M.A. Good, T.V. Bliss, B.T. Hyman, et al. 1999. Impaired synaptic plasticity and learning in aged amyloid precursor

protein transgenic mice. *Nat. Neurosci.* 2:271–276. http://dx.doi.org/10.1038/6374

Chen, D., H. Xiao, K. Zhang, B. Wang, Z. Gao, Y. Jian, X. Qi, J. Sun, L. Miao, and C. Yang. 2010. Retromer is required for apoptotic cell clearance by phagocytic receptor recycling. *Science*. 327:1261–1264. http://dx.doi.org/10.1126/science.1184840

Eaton, S. 2008. Retromer retrieves wntless. *Dev. Cell*. 14:4–6. http://dx.doi.org/10.1016/j.devcel.2007.12.014

Esler, W.P., and M.S. Wolfe. 2001. A portrait of Alzheimer secretases—new features and familiar faces. *Science*. 293:1449–1454. http://dx.doi.org/10.1126/science.1064638

Fitzjohn, S.M., R.A. Morton, F. Kuenzi, T.W. Rosahl, M. Shearman, H. Lewis, D. Smith, D.S. Reynolds, C.H. Davies, G.L. Collingridge, and G.R. Seabrook. 2001. Age-related impairment of synaptic transmission but normal long-term potentiation in transgenic mice that overexpress the human APP695SWE mutant form of amyloid precursor protein. *J. Neurosci.* 21:4691–4698.

Franch-Marro, X., F. Wendler, S. Guidato, J. Griffith, A. Baena-Lopez, N. Itasaki, M.M. Maurice, and J.P. Vincent. 2008. Wingless secretion requires endosome-to-Golgi retrieval of Wntless/Evi/Sprinter by the retromer complex. *Nat. Cell Biol.* 10:170–177. http://dx.doi.org/10.1038/ncb1678

Fukumoto, H., B.S. Cheung, B.T. Hyman, and M.C. Irizarry. 2002. Beta-secretase protein and activity are increased in the neocortex in Alzheimer disease. *Arch. Neurol.* 59:1381–1389. http://dx.doi.org/10.1001/archneur.59.9.1381

Good, M.A., and G. Hale. 2007. The "Swedish" mutation of the amyloid precursor protein (APPswe) dissociates components of object-location memory in aged Tg2576 mice. *Behav. Neurosci.* 121:1180–1191. http://dx.doi.org/10.1037/0735-7044.121.6.1180

Haass, C., C.A. Lemere, A. Capell, M. Citron, P. Seubert, D. Schenk, L. Lannfelt, and D.J. Selkoe. 1995. The Swedish mutation causes early-onset Alzheimer's disease by beta-secretase cleavage within the secretory pathway. *Nat. Med.* 1:1291–1296. http://dx.doi.org/10.1038/nm1295-1291

Hardy, J., and D.J. Selkoe. 2002. The amyloid hypothesis of Alzheimer's disease: Progress and problems on the road to therapeutics. *Science*. 297:353–356. http://dx.doi.org/10.1126/science.1072994

He, X., G. Zhu, G. Koelsch, K.K. Rodgers, X.C. Zhang, and J. Tang. 2003. Biochemical and structural characterization of the interaction of memapsin 2 (beta-secretase) cytosolic domain with the VHS domain of GGA proteins. *Biochemistry*. 42:12174–12180. http://dx.doi.org/10.1021/bi035199h

Hsiao, K., P. Chapman, S. Nilsen, C. Eckman, Y. Harigaya, S. Younkin, F. Yang, and G. Cole. 1996. Correlative memory deficits, Abeta elevation, and amyloid plaques in transgenic mice. *Science*. 274:99–102. http://dx.doi.org/10.1126/science.274.5284.99

Hu, X., X. Zhou, W. He, J. Yang, W. Xiong, P. Wong, C.G. Wilson, and R. Yan. 2010. BACE1 deficiency causes altered neuronal activity and neurodegeneration. *J. Neurosci.* 30:8819–8829. http://dx.doi.org/10.1523/JNEUROSCI.1334-10.2010

Hussain, I., D. Powell, D.R. Howlett, D.G. Tew, T.D. Meek, C. Chapman, I.S. Gloger, K.E. Murphy, C.D. Southan, D.M. Ryan, et al. 1999. Identification of a novel aspartic protease (Asp 2) as beta-secretase. *Mol. Cell. Neurosci.* 14:419–427. http://dx.doi.org/10.1006/mcne.1999.0811

Iwaki, T., A. Hosomi, S. Tokudomi, Y. Kusunoki, Y. Fujita, Y. Giga-Hama, N. Tanaka, and K. Takegawa. 2006. Vacuolar protein sorting receptor in *Schizosaccharomyces pombe*. *Microbiology*. 152:1523–1532. http://dx.doi.org/10.1099/mic.0.28627-0

Jacobsen, J.S., C.C. Wu, J.M. Redwine, T.A. Comery, R. Arias, M. Bowlby, R. Martone, J.H. Morrison, M.N. Pangalos, P.H. Reinhart, and F.E. Bloom. 2006. Early-onset behavioral and synaptic deficits in a mouse model of Alzheimer's disease. *Proc. Natl. Acad. Sci. USA*. 103:5161–5166. http://dx.doi.org/10.1073/pnas.0600948103

Johnson-Wood, K., M. Lee, R. Motter, K. Hu, G. Gordon, R. Barbour, K. Khan, M. Gordon, H. Tan, D. Games, et al. 1997. Amyloid precursor protein processing and A beta42 deposition in a transgenic mouse model of Alzheimer disease. *Proc. Natl. Acad. Sci. USA*. 94:1550–1555. http://dx.doi.org/10.1073/pnas.94.4.1550

Kim, E., Y. Lee, H.J. Lee, J.S. Kim, B.S. Song, J.W. Huh, S.R. Lee, S.U. Kim, S.H. Kim, Y. Hong, et al. 2010. Implication of mouse Vps26b-Vps29-Vps35 retromer complex in sortilin trafficking. *Biochem. Biophys. Res. Commun.* 403:167–171. http://dx.doi.org/10.1016/j.bbrc.2010.10.121

Laird, F.M., H. Cai, A.V. Savonenko, M.H. Farah, K. He, T. Melnikova, H. Wen, H.C. Chiang, G. Xu, V.E. Koliatsos, et al. 2005. BACE1, a major determinant of selective vulnerability of the brain to amyloid-beta amyloidogenesis, is essential for cognitive, emotional, and synaptic functions. *J. Neurosci.* 25:11693–11709. http://dx.doi.org/10.1523/JNEUROSCI.2766-05.2005

Lane, R.F., S.M. Raines, J.W. Steele, M.E. Ehrlich, J.A. Lah, S.A. Small, R.E. Tanzi, A.D. Attie, and S. Gandy. 2010. Diabetes-associated SorCS1 regulates Alzheimer's amyloid-beta metabolism: Evidence for involvement of SorL1 and the retromer complex. *J. Neurosci.* 30:13110–13115. http://dx.doi.org/10.1523/JNEUROSCI.3872-10.2010

Lee, D.H., L.J. Zhou, Z. Zhou, J.X. Xie, J.U. Jung, Y. Liu, C.X. Xi, L. Mei, and W.C. Xiong. 2010. Neogenin inhibits HJV secretion and regulates BMP-induced hepcidin expression and iron homeostasis. *Blood*. 115:3136–3145. http://dx.doi.org/10.1182/blood-2009-11-251199

Li, S., S. Hong, N.E. Shepardson, D.M. Walsh, G.M. Shankar, and D. Selkoe. 2009. Soluble oligomers of amyloid Beta protein facilitate hippocampal long-term depression by disrupting neuronal glutamate uptake. *Neuron*. 62:788–801. http://dx.doi.org/10.1016/j.neuron.2009.05.012

Luo, Y., B. Bolon, S. Kahn, B.D. Bennett, S. Babu-Khan, P. Denis, W. Fan, H. Kha, J. Zhang, Y. Gong, et al. 2001. Mice deficient in BACE1, the Alzheimer's beta-secretase, have normal phenotype and abolished beta-amyloid generation. *Nat. Neurosci.* 4:231–232. http://dx.doi.org/10.1038/85059

Middei, S., S. Daniele, A. Caprioli, O. Ghirardi, and M. Ammassari-Teule. 2006. Progressive cognitive decline in a transgenic mouse model of Alzheimer's disease overexpressing mutant hAPPswe. *Genes Brain Behav.* 5:249–256. http://dx.doi.org/10.1111/j.1601-183X.2005.00160.x

Morris, R.G. 1991. Distinctive computations and relevant associative processes: Hippocampal role in processing, retrieval, but not storage of allocentric spatial memory. *Hippocampus*. 1:287–290. http://dx.doi.org/10.1002/hipo.450010318

Muhammad, A., I. Flores, H. Zhang, R. Yu, A. Staniszewski, E. Planel, M. Herman, L. Ho, R. Kreber, L.S. Honig, et al. 2008. Retromer deficiency observed in Alzheimer's disease causes hippocampal dysfunction, neurodegeneration, and Abeta accumulation. *Proc. Natl. Acad. Sci. USA*. 105:7327–7332. http://dx.doi.org/10.1073/pnas.0802545105

Nimmrich, V., C. Grimm, A. Draguhn, S. Barghorn, A. Lehmann, H. Schoemaker, H. Hillen, G. Gross, U. Ebert, and C. Bruehl. 2008. Amyloid beta oligomers (A beta(1-42) globulomer) suppress spontaneous synaptic activity by inhibition of P/Q-type calcium currents. *J. Neurosci.* 28:788–797. http://dx.doi.org/10.1523/JNEUROSCI.4771-07.2008

Ohno, M., E.A. Sametsky, L.H. Younkin, H. Oakley, S.G. Younkin, M. Citron, R. Vassar, and J.F. Disterhoft. 2004. BACE1 deficiency rescues memory deficits and cholinergic dysfunction in a mouse model of Alzheimer's disease. *Neuron*. 41:27–33. http://dx.doi.org/10.1016/S0896-6273(03)00810-9

Okada, H., W. Zhang, C. Peterhoff, J.C. Hwang, R.A. Nixon, S.H. Ryu, and T.W. Kim. 2010. Proteomic identification of sorting nexin 6 as a negative regulator of BACE1-mediated APP processing. *FASEB J.* 24:2783–2794. http://dx.doi.org/10.1096/fj.09-146357

Pan, C.L., P.D. Baum, M. Gu, E.M. Jorgensen, S.G. Clark, and G. Garriga. 2008. *C. elegans* AP-2 and retromer control Wnt signaling by regulating mig-14/Wntless. *Dev. Cell*. 14:132–139. http://dx.doi.org/10.1016/j.devcel.2007.12.001

Port, F., M. Kuster, P. Herr, E. Furger, C. Bänziger, G. Hausmann, and K. Basler. 2008. Wingless secretion promotes and requires retromer-dependent cycling of Wntless. *Nat. Cell Biol.* 10:178–185. http://dx.doi.org/10.1038/ncb1687

Reed, M.N., P. Liu, L.A. Kotilinek, and K.H. Ashe. 2010. Effect size of reference memory deficits in the Morris water maze in Tg2576 mice. *Behav. Brain Res.* 212:115–120. http://dx.doi.org/10.1016/j.bbr.2010.03.037

Ren, X.R., G.L. Ming, Y. Xie, Y. Hong, D.M. Sun, Z.Q. Zhao, Z. Feng, Q. Wang, S. Shim, Z.F. Chen, et al. 2004. Focal adhesion kinase in netrin-1 signaling. *Nat. Neurosci.* 7:1204–1212. http://dx.doi.org/10.1038/nn1330

Rockenstein, E., L. Crews, and E. Masliah. 2007. Transgenic animal models of neurodegenerative diseases and their application to treatment development. *Adv. Drug Deliv. Rev.* 59:1093–1102. http://dx.doi.org/10.1016/j.addr.2007.08.013

Rogaeva, E., Y. Meng, J.H. Lee, Y. Gu, T. Kawarai, F. Zou, T. Katayama, C.T. Baldwin, R. Cheng, H. Hasegawa, et al. 2007. The neuronal sortilin-related receptor SORL1 is genetically associated with Alzheimer disease. *Nat. Genet.* 39:168–177. http://dx.doi.org/10.1038/ng1943

Roselli, F., M. Tirard, J. Lu, P. Hutzler, P. Lamberti, P. Livrea, M. Morabito, and O.F. Almeida. 2005. Soluble beta-amyloid1-40 induces NMDA-dependent degradation of postsynaptic density-95 at glutamatergic synapses. *J. Neurosci.* 25:11061–11070. http://dx.doi.org/10.1523/JNEUROSCI.3034-05.2005

Seaman, M.N. 2005. Recycle your receptors with retromer. *Trends Cell Biol.* 15:68–75. http://dx.doi.org/10.1016/j.tcb.2004.12.004

Selkoe, D.J. 2002a. Alzheimer's disease is a synaptic failure. *Science*. 298:789–791. http://dx.doi.org/10.1126/science.1074069

Selkoe, D.J. 2002b. Deciphering the genesis and fate of amyloid beta-protein yields novel therapies for Alzheimer disease. *J. Clin. Invest.* 110:1375–1381.

Selkoe, D.J. 2008. Soluble oligomers of the amyloid beta-protein impair synaptic plasticity and behavior. *Behav. Brain Res.* 192:106–113. http://dx.doi.org/10.1016/j.bbr.2008.02.016

Selkoe, D.J., and M.S. Wolfe. 2007. Presenilin: Running with scissors in the membrane. *Cell*. 131:215–221. http://dx.doi.org/10.1016/j.cell.2007.10.012

Selkoe, D.J., T. Yamazaki, M. Citron, M.B. Podlisny, E.H. Koo, D.B. Teplow, and C. Haass. 1996. The role of APP processing and trafficking pathways in the formation of amyloid beta-protein. *Ann. NY Acad. Sci.* 777:57–64. http://dx.doi.org/10.1111/j.1749-6632.1996.tb34401.x

Sinha, S., J.P. Anderson, R. Barbour, G.S. Basi, R. Caccavello, D. Davis, M. Doan, H.F. Dovey, N. Frigon, J. Hong, et al. 1999. Purification and cloning of amyloid precursor protein beta-secretase from human brain. *Nature*. 402:537–540. http://dx.doi.org/10.1038/990114

Sisodia, S.S., and P.H. St George-Hyslop. 2002. gamma-Secretase, Notch, Abeta and Alzheimer's disease: Where do the presenilins fit in? *Nat. Rev. Neurosci.* 3:281–290. http://dx.doi.org/10.1038/nrn785

Small, S.A., K. Kent, A. Pierce, C. Leung, M.S. Kang, H. Okada, L. Honig, J.P. Vonsattel, and T.W. Kim. 2005. Model-guided microarray implicates the retromer complex in Alzheimer's disease. *Ann. Neurol.* 58:909–919. http://dx.doi.org/10.1002/ana.20667

Smith, D.G., R. Cappai, and K.J. Barnham. 2007. The redox chemistry of the Alzheimer's disease amyloid beta peptide. *Biochim. Biophys. Acta*. 1768:1976–1990. http://dx.doi.org/10.1016/j.bbamem.2007.02.002

Stefani, M., and G. Liguri. 2009. Cholesterol in Alzheimer's disease: Unresolved questions. *Curr. Alzheimer Res.* 6:15–29. http://dx.doi.org/10.2174/156720509787313899

Tanzi, R.E., and L. Bertram. 2005. Twenty years of the Alzheimer's disease amyloid hypothesis: A genetic perspective. *Cell*. 120:545–555. http://dx.doi.org/10.1016/j.cell.2005.02.008

Thinakaran, G., and E.H. Koo. 2008. Amyloid precursor protein trafficking, processing, and function. *J. Biol. Chem.* 283:29615–29619. http://dx.doi.org/10.1074/jbc.R800019200

Townsend, M., G.M. Shankar, T. Mehta, D.M. Walsh, and D.J. Selkoe. 2006. Effects of secreted oligomers of amyloid beta-protein on hippocampal synaptic plasticity: A potent role for trimers. *J. Physiol.* 572:477–492. http://dx.doi.org/10.1113/jphysiol.2005.103754

van Weering, J.R., P. Verkade, and P.J. Cullen. 2010. SNX-BAR proteins in phosphoinositide-mediated, tubular-based endosomal sorting. *Semin. Cell Dev. Biol.* 21:371–380. http://dx.doi.org/10.1016/j.semcdb.2009.11.009

Vassar, R., B.D. Bennett, S. Babu-Khan, S. Kahn, E.A. Mendiaz, P. Denis, D.B. Teplow, S. Ross, P. Amarante, R. Loeloff, et al. 1999. Beta-secretase cleavage of Alzheimer's amyloid precursor protein by the transmembrane aspartic protease BACE. *Science*. 286:735–741. http://dx.doi.org/10.1126/science.286.5440.735

Vassar, R., D.M. Kovacs, R. Yan, and P.C. Wong. 2009. The beta-secretase enzyme BACE in health and Alzheimer's disease: Regulation, cell biology, function, and therapeutic potential. *J. Neurosci.* 29:12787–12794. http://dx.doi.org/10.1523/JNEUROSCI.3657-09.2009

Vilariño-Güell, C., C. Wider, O.A. Ross, J.C. Dachsel, J.M. Kachergus, S.J. Lincoln, A.I. Soto-Ortolaza, S.A. Cobb, G.J. Wilhoite, J.A. Bacon, et al. 2011. VPS35 mutations in Parkinson disease. *Am. J. Hum. Genet.* 89:162–167. http://dx.doi.org/10.1016/j.ajhg.2011.06.001

Walsh, D.M., I. Klyubin, G.M. Shankar, M. Townsend, J.V. Fadeeva, V. Betts, M.B. Podlisny, J.P. Cleary, K.H. Ashe, M.J. Rowan, and D.J. Selkoe. 2005. The role of cell-derived oligomers of Abeta in Alzheimer's disease and avenues for therapeutic intervention. *Biochem. Soc. Trans.* 33:1087–1090. http://dx.doi.org/10.1042/BST20051087

Wen, L., Y.S. Lu, X.H. Zhu, X.M. Li, R.S. Woo, Y.J. Chen, D.M. Yin, C. Lai, A.V. Terry Jr., A. Vazdarjanova, et al. 2010. Neuregulin 1 regulates pyramidal neuron activity via ErbB4 in parvalbumin-positive interneurons. *Proc. Natl. Acad. Sci. USA*. 107:1211–1216. http://dx.doi.org/10.1073/pnas.0910302107

Willnow, T.E., A.S. Carlo, M. Rohe, and V. Schmidt. 2010. SORLA/SORL1, a neuronal sorting receptor implicated in Alzheimer's disease. *Rev. Neurosci.* 21:315–329. http://dx.doi.org/10.1515/REVNEURO.2010.21.4.315

Xie, Y., Y.Q. Ding, Y. Hong, Z. Feng, S. Navarre, C.X. Xi, X.J. Zhu, C.L. Wang, S.L. Ackerman, D. Kozlowski, et al. 2005. Phosphatidylinositol transfer protein-alpha in netrin-1-induced PLC signalling and neurite outgrowth. *Nat. Cell Biol.* 7:1124–1132. http://dx.doi.org/10.1038/ncb1321

Yan, R., M.J. Bienkowski, M.E. Shuck, H. Miao, M.C. Tory, A.M. Pauley, J.R. Brashier, N.C. Stratman, W.R. Mathews, A.E. Buhl, et al. 1999. Membrane-anchored aspartyl protease with Alzheimer's disease beta-secretase activity. *Nature*. 402:533–537. http://dx.doi.org/10.1038/990107

Yang, L.B., K. Lindholm, R. Yan, M. Citron, W. Xia, X.L. Yang, T. Beach, L. Sue, P. Wong, D. Price, et al. 2003. Elevated beta-secretase expression and enzymatic activity detected in sporadic Alzheimer disease. *Nat. Med.* 9:3–4. http://dx.doi.org/10.1038/nm0103-3

Yang, P.T., M.J. Lorenowicz, M. Silhankova, D.Y. Coudreuse, M.C. Betist, and H.C. Korswagen. 2008. Wnt signaling requires retromer-dependent recycling of MIG-14/Wntless in Wnt-producing cells. *Dev. Cell*. 14:140–147. http://dx.doi.org/10.1016/j.devcel.2007.12.004

Zha, Q., Y. Ruan, T. Hartmann, K. Beyreuther, and D. Zhang. 2004. GM1 ganglioside regulates the proteolysis of amyloid precursor protein. *Mol. Psychiatry*. 9:946–952. http://dx.doi.org/10.1038/sj.mp.4001509

Zhou, Z., J. Xie, D. Lee, Y. Liu, J. Jung, L. Zhou, S. Xiong, L. Mei, and W.C. Xiong. 2010. Neogenin regulation of BMP-induced canonical Smad signaling and endochondral bone formation. *Dev. Cell*. 19:90–102. http://dx.doi.org/10.1016/j.devcel.2010.06.016

Zhu, X.J., C.Z. Wang, P.G. Dai, Y. Xie, N.N. Song, Y. Liu, Q.S. Du, L. Mei, Y.Q. Ding, and W.C. Xiong. 2007. Myosin X regulates netrin receptors and functions in axonal path-finding. *Nat. Cell Biol.* 9:184–192. http://dx.doi.org/10.1038/ncb1535

Zimprich, A., A. Benet-Pagès, W. Struhal, E. Graf, S.H. Eck, M.N. Offman, D. Haubenberger, S. Spielberger, E.C. Schulte, P. Lichtner, et al. 2011. A mutation in VPS35, encoding a subunit of the retromer complex, causes late-onset Parkinson disease. *Am. J. Hum. Genet.* 89:168–175. http://dx.doi.org/10.1016/j.ajhg.2011.06.008